The *Trypanosoma brucei* Cytoskeletal Protein KHARON Associates with Partner Proteins to Mediate Both Cytokinesis and Trafficking of Flagellar Membrane Proteins

Marco A. Sanchez, and Scott M. Landfear*

Department of Molecular Microbiology & Immunology, Oregon Health & Science University, Portland, Oregon, USA

*Author for correspondence (landfear@ohsu.edu)

Summary Statement: This study investigates the essential role in African trypanosomes of the KHARON protein and its molecular partners in trafficking of membrane proteins to the flagellum.

ABSTRACT

In the African trypanosome *Trypanosoma brucei*, the cytoskeletal protein *Tb*KHARON is required for trafficking of a putative Ca^{2+} channel to the flagellar membrane, and it is essential for parasite viability in both the mammalian stage bloodstream forms and the tsetse fly procyclic forms. This protein is located at the base of the flagellum, in the pellicular cytoskeleton, and in the mitotic spindle in both life cycle forms, and it likely serves multiple functions for these parasites. To begin to deconvolve the functions of KHARON, we have investigated partners associated with this protein and their roles in parasite biology. One KHARON associated protein, *Tb*KHAP1, is a close interaction partner that can be crosslinked to KHARON by formaldehyde and pulled down in a molecular complex, and it colocalizes with *Tb*KHARON at the base of the flagellum. Knockdown of *TbKHAP1* mRNA has similar phenotypes to knockdown of its partner *Tb*KHARON, impairing trafficking of the Ca^{2+} channel to the flagellar membrane and blocking cytokinesis, implying that the *Tb*KHARON/*Tb*KHAP1 complex mediates trafficking of flagellar membrane proteins. Two other KHAPs, *Tb*KHAP2 and *Tb*KHAP3, are in close proximity to *Tb*KHARON but may not be direct interaction partners, and knockdown of their mRNAs does not affect trafficking of the Ca^{2+} channel. Two different flagellar membrane proteins, which are extruded from the flagellar membrane into extracellular vesicles, are also dependent upon *Tb*KHARON for flagellar trafficking. These studies confirm that *Tb*KHARON acts in complexes with other proteins to carry out various biological functions, and that some partners are involved in the core activity of targeting membrane proteins to the flagellum.

KEYWORDS *Trypanosoma brucei*, cytoskeleton, cytokinesis, flagellar membrane protein trafficking, protein complexes, virulence

INTRODUCTION

African trypanosomes of the species *Trypanosoma brucei* are parasitic protists that cause human African trypanosomiasis and the disease nagana in cattle and are thus of great medical and veterinary importance (Kennedy, 2013). In addition, these parasites have been recognized as valuable models for probing fundamental questions in cell and molecular biology (Cayla et al., 2019). *T. brucei* and related kinetoplastid parasites such as *Trypanosoma cruzi* and *Leishmania* species are flagellated and offer novel insights into the structure and function of flagella (Langousis and Hill, 2014) and the roles of these organelles in infection (Kelly et al., 2020a). Furthermore, the cell division cycle of African trypanosomes has been studied extensively (Farr and Gull, 2012; Vaughan and Gull, 2008; Wheeler et al., 2019), identifying various processes that are important for both proliferative and differentiation-linked cell division.

In previous work on trafficking of integral membrane proteins to flagella, we identified a kinetoplastid-specific protein designated KHARON (KH) that plays a critical role in flagellar targeting of the putative Ca^{2+} channel *Tb*CaCh (Tb927.10.2880) in *T. brucei*, originally identified as a flagellar surface protein FS179 (Oberholzer et al., 2011), and the flagellar glucose transporter *Lmx*GT1 in *L. mexicana* (Tran et al., 2013) (see Table S1 for tabulation of gene IDs and names of *T. brucei* proteins investigated in this study). In both species of parasite (Sanchez et al., 2016), KHARON was localized to three distinct subcellular compartments: the base of the flagellum (Fig. 1A), the subpellicular microtubules that subtend the plasma membrane around the cell body, and the mitotic spindle (Fig. 1B). Application of RNA interference (RNAi) to knock down *TbKH* (Tb927.10.8940) revealed that, in addition to preventing flagellar trafficking of *Tb*CaCh/FS179, the flagellum attachment zone (FAZ) was disrupted, resulting in detachment of flagella from the cell body (Sanchez et al., 2016), leaving this organelle adherent only through its connection at the flagellar pocket. Interfering with trafficking of *Tb*CaCh/FS179 to the flagellar membrane is likely to induce disruption of flagellar attachment, as RNAi directed against this channel also results in a similar flagellar detachment phenotype (Oberholzer et al., 2011). In addition, as found for many genetic alterations that disrupt flagellar attachment, these parasites are unable to initiate cell division, generating trypanosomes in which nuclei, kinetoplasts (mitochondrial DNA-containing structures), basal bodies, and flagella have replicated but cytokinesis has not occurred. This phenotype was apparent in both mammalian bloodstream form (BF) and insect stage procyclic form (PF) parasites and was thus lethal to both life cycle stages.

Similar studies in *L. mexicana* have also established a critical role for *Lmx*KH (LmxM.36.5850) in the life cycle of *Leishmania* parasites. Thus a Δ*lmxkh* null mutant was generated in insect stage promastigotes, where trafficking of *Lmx*GT1 to the flagellum was strongly impaired (Tran et al.,

81 2013), but cell division and replication of this life cycle stage was not affected. In contrast, Δ*lmxkh*
82 null mutants were unable to undergo cytokinesis after invading host macrophages, resulting in
83 formation of multinucleate multiflagellated amastigotes that died over the course of several days
84 (Tran et al., 2013). These null mutants were also avirulent following injection into BALB/c mice
85 (Tran et al., 2015), and studies by others have shown that *KHARON* null mutants in *L. infantum*
86 have potential as a live attenuated vaccine (Santi et al., 2018).

87 KHARON exhibits both similarities and striking differences between *T. brucei* (*Tb*KH) and *L.*
88 *mexicana* (*Lmx*KH). Thus, the two orthologs are relatively divergent in sequence, sharing 27%
89 amino acid identity and differing significantly in length (411 amino acids for *Tb*KH versus 520
90 amino acids for *Lmx*KH). *Tb*KH is critical for cell division of both mammalian BF and insect stage
91 PF parasites, whereas *Lmx*KH is only essential for division of disease-causing amastigotes.
92 Nonetheless, the three subcellular locations for KHARON are shared between the two parasites,
93 as are functions in cytokinesis and formation of the flagellar membrane.

94 KHARON proteins do not share significant sequence similarity to proteins outside the
95 Kinetoplastida, nor do they contain conserved sequence motifs that are suggestive of specific
96 biochemical or cellular functions. Furthermore, their residence at multiple subcellular locations
97 suggests that KHARON proteins are likely to be multifunctional, participating in flagellar
98 membrane trafficking, cytokinesis, and spindle function. Additionally, it is possible that distinctions
99 in function could be conferred by association of KHARON with different partner proteins at each
100 of its three subcellular loci. Thus, we hypothesize that there could exist three distinct KHARON
101 Complexes, Complex 1 at the base of the flagellum, Complex 2 at the subpellicular cytoskeleton,
102 and Complex 3 at the mitotic spindle. Furthermore, given the apparent differences in *Tb*KH and
103 *Lmx*KH noted above, there may be similarities and differences between these putative complexes
104 between the two species of parasite.

105 To initiate a study of putative KHARON Complexes and their functions, we carried out
106 biotinylation proximity labeling (BioID) (Roux et al., 2012) and tandem affinity purification-mass
107 spectrometry (TAP-MS) (Kaiser et al., 2008) on *Lmx*KH, resulting in the identification of two
108 KHARON Associated Proteins, *Lmx*KHAP1 and *Lmx*KHAP2 (LmxM.32.2440 and LmxM.05.0380,
109 respectively; (Kelly et al., 2020b)). In parallel, we investigated these two KHARON partners in *T.*
110 *brucei* and report the results of those studies here. As anticipated, *Tb*KHAP1 and *Tb*KHAP2
111 exhibit both similarities and notable differences compared to their orthologs in *L. mexicana*. In
112 addition, *T. brucei* expresses another KHARON partner related to *Tb*KHAP2 that we designate
113 *Tb*KHAP3. Furthermore, characterization of additional flagellar membrane proteins suggests that
114 *Tb*KH expression is important for flagellar targeting of multiple such proteins in African

115 trypanosomes, whereas the role of *Lmx*KH in trafficking of flagellar membrane proteins appears
116 to be more restricted. These studies confirm that KHARON proteins in both parasites exist in
117 complexes with various partners and that these partner proteins can play distinct roles in the
118 functions of different KHARON Complexes.
119

120 **RESULTS**

121 **Localization of *Tb*KHAP1, *Tb*KHAP2, TbKHAP3, and *Tb*KH in bloodstream and**
122 **procyclic African trypanosomes.** To facilitate studies on *Tb*KH and its partners, we raised and
123 affinity purified a polyclonal antibody against this protein, anti-*T*bKH pAb. Western blot analysis
124 indicated that anti-*Tb*KH pAb detects a single protein of ~49 kDa molecular weight, and that an
125 additional band of ~62 kDa appears in parasites also expressing a BirA* fusion on the N-terminus
126 of *T*bKH (Fig. 1 C), establishing that this antibody is of suitable specificity to employ in localization
127 and biochemical characterization of *Tb*KH. To determine whether *Tb*KHAP1 (Tb927.11.2610),
128 *Tb*KHAP2 (Tb927.10.10360) and *Tb*KHAP3 (Tb927.10.10280) are associated with *Tb*KH in a
129 complex, several complementary approaches were applied. First, each KHAP was tagged at its
130 N-terminus with the triple hemagglutinin peptide tag HA_3, and formaldehyde-fixed BF and PF
131 trypanosomes were examined by immunofluorescence deconvolution microscopy (Fig. 2).
132 HA_3::*Tb*KHAP1 (Fig. 2A,B, green) overlaps with *Tb*KH (red) at the cell periphery, as demonstrated
133 by the yellow color in this region of both BF and PF parasites. In contrast, there was no apparent
134 overlap of the two signals in the mitotic spindle (central red oval or line marked with a white arrow),
135 indicating that this protein could be associated with *Tb*KH in the subpellicular cytoskeleton but not
136 at the mitotic spindle. Similarly, *Tb*KHAP2::HA_3 (Figs. 2C,D) and $V5_3$::*Tb*KHAP3 or
137 HA_3::*Tb*KHAP3 (Fig. 2E,F) overlap with *Tb*KH at the cell periphery but not at the mitotic spindle.
138 For each of the *Tb*KHAPs, there is also green fluorescence that does not coincide with *Tb*KH so
139 that there is not complete overlap of the signals, and there may thus be populations of each
140 protein that are not associated with each other. However overall, these three *Tb*KHAPs are
141 candidates for *Tb*KH partners that are selective for the subpellicular cytoskeleton versus the
142 mitotic spindle.

143 To determine whether *Tb*KHAP1, *Tb*KHAP2, or *Tb*KHAP3 might associate with *Tb*KH at the
144 base of the flagellum, flagella were isolated from parasites expressing each HA_3- or $V5_3$-tagged
145 *Tb*KHAP and imaged by deconvolution microscopy. Fig. 3 shows that HA_3::*Tb*KHAP1 (Fig. 3A),
146 TbKHAP2::HA_3 (Fig. 3B) and HA_3::TbKHAP3 (Fig. 3C) overlap significantly with *Tb*KH in the
147 region of the flagellum immediately adjacent to the kinetoplast DNA (kDNA, blue, Fig. 3A), which
148 is close to and physically attached to (Robinson and Gull, 1991) the flagellar basal body. Overall,
149 these results indicate that *Tb*KHAP1, *Tb*KHAP2, and *Tb*KHAP3 could be partners for *Tb*KH at
150 both the pellicular cytoskeleton and the base of the flagellum. It is noteworthy that *Tb*KHAP3 was
151 previously identified as a basal body protein in a proteomic study of that subcellular structure
152 (Dang et al., 2017). Hence, it is likely that *Tb*KH, *Tb*KHAP1, *Tb*KHAP2, and *Tb*KHAP3 are all
153 basal body components.

154 **Molecular association of *Tb*KHAP1, *Tb*KHAP2, and *Tb*KHAP3 with *Tb*KH.** To determine
155 whether the observed subcellular overlap of the fluorescence signals from *Tb*KHAPs and *Tb*KH
156 could indicate physical association in molecular complexes, *Tb*KH was endogenously tagged at
157 its N-terminus with a His_{10} affinity tag (His_{10}::*Tb*KH) to allow pulldown of this protein, and
158 associated partners, with Co^{2+} agarose resin, and this affinity tagged protein was expressed in a
159 BF cell line also expressing either HA_3::*Tb*KHAP1, *Tb*KHAP2:: HA_3, or $V5_3$::*Tb*KHAP3. Because
160 *Tb*KH is an integral component of the parasite cytoskeleton (Sanchez et al., 2016) and would
161 pulldown many cytoskeletal proteins in an experiment performed under native conditions, we first
162 crosslinked with formaldehyde parasites expressing each pair of tagged proteins. Formaldehyde
163 crosslinks proteins that are in very close proximity (~2-3 Å, reference (Hoffman et al., 2015)), so
164 this treatment will covalently attach close molecular partners of *Tb*KH but not proteins that are
165 more distant partners in a complex or proteins that are in the cytoskeleton but distant from *Tb*KH.
166 Subsequent treatment with strongly denaturing reagents will dissociate peripheral proteins from
167 His_{10}::*Tb*KH while retaining crosslinked partners, and the closely associated partners will thus be
168 purified along with His_{10}::*Tb*KH, following binding and elution from Co^{2+} resin, and released upon
169 heat-induced reversal of the crosslinks.
170 Fig. 4A demonstrates that HA_3::*Tb*KHAP1 is pulled down with His_{10}::*Tb*KH when parasites are
171 formaldehyde crosslinked (EF*) but not when they are not subjected to crosslinking (EF). As a
172 negative control, another subpellicular cytoskeletal protein, CAP15 (Vedrenne et al., 2002), was
173 HA_3 tagged and expressed in His_{10}::*Tb*KH expressing BF parasites, but this protein was not pulled
174 down even from formaldehyde-crosslinked parasites. Parallel experiments were performed using
175 BF parasites expressing *Tb*KHAP2::HA_3, or $V5_3$::*Tb*KHAP3 and His_{10}::*Tb*KH. Despite extensive
176 efforts, we have not been able to observe pulldowns of either tagged protein with His_{10}::*Tb*KH,
177 raising the possibility that these proteins are not in close enough contact to *Tb*KH to crosslink.
178 These experiments establish that *Tb*KHAP1 is in very close proximity to *Tb*KH and these two
179 proteins are thus molecular partners.
180 **Proximity ligation assay (PLA) confirms close proximity of *Tb*KH with *Tb*KHAP1,**
181 ***Tb*KHAP2, and *Tb*KHAP3.** To provide another independent examination of whether *Tb*KH is in
182 close physical proximity with each *Tb*KHAP, we performed the PLA in parasites expressing
183 HA_3::*Tb*KHAP1, *Tb*KHAP2::HA_3, and HA_3::*Tb*KHAP3. In this assay (Fredriksson et al., 2002;
184 Soderberg et al., 2006), cells expressing two partner proteins are first reacted with primary
185 antibodies from different species. Parasites are subsequently incubated with species-specific
186 secondary antibodies directed against each primary antibody, and each of these secondary
187 antibodies contains a unique, covalently attached oligonucleotide. Only if the two target proteins

188 are within ~400 Å of each other, these oligonucleotides can base pair to another linker
189 oligonucleotide and be covalently ligated into a circular substrate that can participate in rolling
190 circle DNA amplification of the cognate sequence. The amplified sequence is then hybridized to
191 a fluorescently labeled DNA probe, resulting in fluorescent puncta within the cell.

192 Fig. 4B,C shows a positive PLA signal (left panels) for BF and PF trypanosomes expressing
193 HA_3::*Tb*KHAP1 and probed with anti-*Tb*KH rabbit and anti-HA murine mAb. In contrast, when the
194 anti-*Tb*KH antibody is not employed (right panels), the PLA signal is absent, demonstrating the
195 dependency of the signal on detection of both closely associated proteins. Similar results confirm
196 that *Tb*KH is in close physical proximity to *Tb*KHAP2 (Fig. 4D,E) and *Tb*KHAP3 (Fig. 4F,G).

197 **Predicted properties of *Tb*KHAP1, *Tb*KHAP2, and *Tb*KHAP3.** Bioinformatic analysis of the
198 50.9 kDa *Tb*KHAP1 sequence indicates that it is a protein apparently unique to kinetoplastid
199 protists for which there are orthologs widely distributed among Kinetoplastida. A BLASTP search
200 (tritrypdb.org) revealed several coiled-coil proteins such as neurofilament proteins and
201 tropomyosin as being significantly, although not closely, related (E values of 2.6e-08 – 5.4e-12).
202 Prediction of protein disorder using the PrDOS web server (Ishida and Kinoshita, 2007)
203 (http://prdos.hgc.jp/cgi-bin/top.cgi) generated a strong prediction of disorder (probability >0.9)
204 over the C-terminal region from amino acids 314 – 461. Indeed, this sequence is rich in E
205 residues, which predispose such regions to intrinsic disorder (Uversky, 2013), and this property
206 suggests that this region could be involved in protein-protein interactions through induced folding
207 (Zhang et al., 2013). InterPro (Mitchell et al., 2015)
208 (https://www.ebi.ac.uk/interpro/search/sequence/) predicted coils between amino acids 7 – 31
209 and 196 – 241 and a disordered region from residue 332 - 461 , and PSIPRED V4.0 (McGuffin et
210 al., 2000) (http://bioinf.cs.ucl.ac.uk/psipred/) predicted the sequence to be largely helix or coil.
211 Overall, computational analyses suggest that TbKHAP1 is a coiled-coil protein with an intrinsically
212 disordered C-terminus, both properties that are consistent with formation of multi-protein
213 complexes.

214 *Tb*KHAP2 is the 374 kDa microtubule-associated repetitive protein 1, MARP-1, and *Tb*KHAP3
215 is the 267 kDa MARP-2 that have been studied previously by Seebeck and colleagues (Affolter
216 et al., 1994; Hemphill et al., 1992; Schneider et al., 1988) and will hereafter be referred to as
217 *Tb*KHAP2/MARP-1 and *Tb*KHAP3/MARP-2 to indicate both their association with *Tb*KH and their
218 previously demonstrated roles in microtubule binding. Each sequence contains short unique N-
219 and C-terminal domains, and the remainder of the sequence consists of 38-amino acid repeats
220 that are largely conserved within each sequence but ~50% identical between the two proteins.
221 The unique C-terminal domains (95% identical between the two proteins) bind to microtubules

222 (Affolter et al., 1994), and the proteins decorate the subpellicular cytoskeleton (Schneider et al.,
223 1988), but their specific biological functions have not been elucidated. In addition, these proteins
224 have also been localized to the basal body and *Tb*KHAP3/MARP-2 was designated *Tb*BBP268
225 (Dang et al., 2017).

226 **Phenotypes of BF trypanosomes following knockdown of *TbKHAP1* RNA.** We have
227 previously demonstrated that knockdown of *TbKH* RNA by inducible RNAi results in a lethal
228 phenotype on both BF and PF trypanosomes (Sanchez et al., 2016). In these parasites, the
229 flagellum detaches from the cell body along the flagellum attachment zone (FAZ), and the
230 parasites are blocked in cytokinesis, resulting in accumulation of multi-nucleated, multi-flagellated
231 'monster cells' that are not viable in the long term. To assess the roles of *Tb*KHAP1,
232 *Tb*KHAP2/MARP-1, and *Tb*KHAP3/MARP-2 in the biology of BF parasites, we targeted by
233 RNAi *TbKHAP1* mRNA, using a unique RNAi probe, and *TbKHAP2/TbKHAP3* mRNAs jointly,
234 using a 500 nt probe covering the conserved C-termini, and assessed the consequent
235 phenotypes.

236 Induction of RNAi against *Tb*KHAP1 in BFs using doxycycline resulted in rapid reduction in
237 the level of this protein (Fig. 5A). Furthermore, RNAi-induced parasites stopped growing almost
238 immediately and were largely dead by 72 h (Fig. 5B). Quantification via microscopy of the
239 percentage of cells with different numbers of nuclei and kinetoplasts (Fig. 5C) showed that
240 following induction of RNAi over 48 h, the percentage of 1N1K parasites dropped dramatically,
241 while those with multiple nuclei and kinetoplasts (XNYK) increased and began to predominate the
242 population. In comparison to the normal morphology of pre-induced parasites (Fig. 5D), induction
243 of RNAi for 20 h (Fig. 5E) or 48 h (Fig. 5F) resulted in parasites with multiple nuclei and/or
244 kinetoplasts and tadpole-like morphology (white arrowhead) or duplicated flagella located at
245 opposite poles of the cell body (yellow arrowhead).

246 Notable among cells in RNAi induced populations are those with multiple flagella located at
247 various relative positions around the cell (e.g., the two parasites in Fig. 5F). Such parasites have
248 initiated cytokinesis and cleavage furrow formation, as the two duplicated flagella have moved
249 apart from the initial position they would have following flagellar duplication. However, the
250 cleavage furrow did not progress to separate the duplicated nuclei and kinetoplasts as it would in
251 normal cell division. In summary, these observations suggest that loss of *Tb*KHAP1 protein from
252 BF parasites results in a block in progression of cleavage furrow rather than an inability to initiate
253 cleavage furrow ingression.

254 These results are further enhanced by more refined time course studies shown in Fig. S1
255 following the progression of nuclear content and cell morphologies between 0 – 48 h after

256 induction of RNAi against *TbKHAP1* RNA. At 4 h (Fig. S1B) and 8 h (Fig. S1C) most parasites
257 had morphologies similar to that preceding induction of RNAi (0 h, Fig. S1A). However, by 12 h
258 (Fig. S1D), multi-flagellated parasites with ingression furrows appeared, and by 24 h and 48 h
259 (Fig. S1E,F), many parasites had incompletely resolved ingression furrows and multiple nuclei.

260 **Phenotypes of parasites following knockdown of *TbKHAP2/MARP-1* and**
261 ***TbKHAP3/MARP-2* RNAs.** Induction of RNAi jointly against *TbKHAP2/MARP-1* and
262 *TbKHAP3/MARP-2* resulted in complete loss of HA_3::*Tb*KHAP2/MARP-1 protein by 24 h (Fig.
263 6A). Depletion of *Tb*KHAP2/MARP-1 and *Tb*KHAP3/MARP-2 impaired growth of BF parasites,
264 resulting in an ~50-fold reduction in parasite number by 120 h (Fig. 6B) post-induction, but growth
265 inhibition was not nearly as pronounced as it is for *Tb*KHAP1 RNAi (Fig. 5B). Compared to
266 uninduced parasites (Fig. 6C), images of parasites following 4 d RNAi (Fig. 6D) still showed many
267 parasites with normal morphology similar to that of uninduced parasites, but some parasites
268 rounded up and showed multiple flagella (Fig. 6D, white arrowhead, flagella on opposite sides of
269 the cell body in DIC image). By 4 d post-RNAi, parasites with 1N2K and XNYK began to
270 accumulate (Fig. 6E), but the proportion was not nearly as great as for RNAi directed against
271 TbKHAP1 (Fig. 5C).

272 ***Tb*KHAP1, but not *Tb*KHAP2/MARP-1 or *Tb*KHAP3/MARP-2, is required for targeting**
273 ***Tb*CaCh/FS179 to the flagellar membrane.** The observation that *Tb*KHAP1 is located at the
274 base of the flagellum (Fig. 3A), likely in the basal body, raises the question of whether it could
275 play a role in the function of *Tb*KH in mediating trafficking of the putative Ca^{2+} channel,
276 *Tb*CaCh/FS179, to the flagellar membrane. To test this possibility, we induced RNAi against
277 *TbKHAP1* RNA in parasites expressing *Tb*CaCh/FS179::HA_3 tagged at the C-terminus, which
278 localized to the flagellar membrane prior to RNAi (Fig. 7A). BF parasites induced for RNAi for 24
279 h (Fig. 7B) or 48 h (Fig. 7C) exhibited flagella that were devoid of *Tb*CaCh::HA_3 (white
280 arrowheads). These results suggest that a complex of *Tb*KH/*Tb*KHAP1, and potentially other
281 currently unknown partners located at the base of the flagellum, is involved in trafficking this
282 channel to the flagellar membrane. Since both proteins are also located in the subpellicular
283 cytoskeleton, it is not possible to definitively ascribe this flagellar trafficking phenotype to the
284 complex at the base of the flagellum; complexes at both locations will be downregulated by
285 *TbKHAP1* RNAi. However, integral membrane proteins are first delivered to the flagellar pocket
286 membrane during biosynthesis (Manna et al., 2014). Hence, the presence of a protein complex
287 located close to the interface between the flagellar pocket and flagellar membrane, and for which
288 downregulation of both known partners inhibits trafficking of a protein into the flagellar membrane,
289 suggests that this complex may mediate trafficking of *Tb*CaCh/FS179 from the flagellar pocket

290 membrane into the flagellar membrane. Such trafficking would presumably be mediated by a
291 direct interaction between *Tb*KH and the cargo, *Tb*CaCh/FS179, and such a molecular interaction
292 has been demonstrated to occur (Sanchez et al., 2016).

293 In contrast, RNAi directed against *TbKHAP2/MARP-1* and *TbKHAP3/MARP-2* RNAs did
294 not prevent trafficking of *Tb*CaCh/FS179::HA_3 into the flagellar membrane, where it is located
295 prior to RNAi (Fig. 7D). At both 4 d (Fig. 7E) and 7 d (Fig. 7F) post RNAi, BF parasites with multiple
296 flagella still trafficked this channel into the flagellar membrane (green arrowheads).

297 ***Tb*KH-dependent trafficking of other flagellar membrane proteins.** *Tb*KH is required for
298 trafficking of *Tb*CaCh/FS179 to the flagellar membrane of BF trypanosomes, and the two protein
299 interact with each other, as demonstrated by crosslinking pulldown assays (Sanchez et al., 2016).
300 Is *Tb*KH important for flagellar trafficking of other membrane proteins? To address this question,
301 we monitored the dependency of other flagellar membrane proteins on *Tb*KH for targeting to that
302 organelle. The TrypTag project (http://tryptag.org/) has defined the subcellular location of a large
303 number of trypanosome proteins in PF parasites (Dean et al., 2017), employing live cell
304 microscopy of parasites expressing mNeonGreen fluorescent protein fusions, and this endeavor
305 has identified a cohort of flagellar membrane proteins.

306 One such flagellar membrane protein is Tb927.7.4270, a 25 kDa protein predicted to have a
307 N-terminal signal sequence and a single transmembrane domain (TMD) near its C-terminus. This
308 protein is one of four paralogous proteins (Tb927.7.4230, 4260, 4270, and 4280) studied
309 previously by Shimogawa *et al*. (Shimogawa et al., 2015) and designated the Fam79 proteins
310 (Fam79.1, 79.2, 79.3, and 79.4, respectively). To address potential dependency upon *Tb*KH for
311 flagellar targeting, we monitored the localization of the C-terminal mNG fusion of
312 Tb927.7.4270/Fam97.3 in both formaldehyde fixed and live PF parasites immobilized in CyGEL
313 (MacLean et al., 2013). As shown in Fig. 8A (0 h RNAi), this fusion protein is present in flagella
314 and also in filaments and vesicles that emerge from the flagella, and we designate Tb927.7.4270
315 as extracellular vesicle membrane protein 1 or *Tb*EVMP1/Fam79.3. Multiple investigators have
316 observed filaments and vesicles emerging from various parts of trypanosomes (Baudieri and
317 Tomassini, 1962; Ellis et al., 1976; Molloy and Ormerod, 1964; Schepilewsky, 1912; Vickerman
318 and Luckins, 1969; Wright and Lumsden, 1970), including the flagella, and a recent study by
319 Szempruch *et al*. (Szempruch et al., 2016a; Szempruch et al., 2016b) has investigated such
320 structures from BF parasites in detail and concluded that the flagellum-derived nanotubes and
321 resulting extracellular vesicles (EVs) incorporate a cohort of parasite proteins. Furthermore,
322 delivery of parasite-derived EVs to host red blood cells or to other trypanosomes can mediate
323 pathogenic processes, such as erythrocyte clearance and anemia in the mammalian host or

324 delivery of innate immune factors from a resistant to a sensitive strain of trypanosome. Hence,
325 understanding the process for delivery of parasite proteins to these EVs is of importance for
326 deciphering mechanisms of parasite virulence. Notably, when PF parasites expressing
327 *Tb*EVMP1::mNG were subjected to RNAi directed against *Tb*KH for 24 h, they were strongly
328 impaired in trafficking of this fusion protein to flagella or nanotubes (Fig. 8A, 24 h RNAi), and
329 fluorescence often accumulated within the parasite cell body. White arrows indicate flagella that
330 are devoid of fluorescence and which thus exhibit a trafficking defect. This result indicates that
331 *Tb*EVMP1/Fam79.3 is dependent upon *Tb*KH, either directly or indirectly, for trafficking to the
332 flagellum and subsequently for release into EVs. Furthermore, this trafficking defect occurs after
333 24 h of RNAi directed against *Tb*KH, but these PF parasites do not exhibit significant loss of
334 viability until ~10 days of continuous RNAi (Sanchez et al., 2016), indicating that the effects of
335 *TbKH* RNAi upon flagellar trafficking are not due to global loss of cellular functions. Notably,
336 Fam79.1 (Tb927.7.4230) was also detected by proteomic analysis in EVs of BF trypanosomes by
337 Szempruch *et al*. (Szempruch et al., 2016b), indicating that multiple members of this family are
338 delivered to the membranes of EVs during the parasite life cycle.
339 A second flagellar membrane protein localized in TrypTag is Tb927.11.1830, designated here
340 as *Tb*EVMP2. This 62 kDa protein has 6 predicted TMDs and is widely distributed among the
341 kinetoplastid protists but does not have obvious orthologs outside that order, nor does it possess
342 conserved Pfam domains (Sonnhammer et al., 1998), except for the TMDs and one predicted
343 coiled coil. The *Tb*EVMP2::mNG fusion protein is also localized to the flagellar membrane,
344 nanotubes, and extracellular vesicles in PF parasites (Fig. 8B, 0 h RNAi), but induction of RNAi
345 directed against *Tb*KH also inhibits trafficking to these flagellar structures (Fig. 8B, 24 h RNAi),
346 albeit less strongly than for *Tb*EVMP1. Although fluorescence is visible in some flagella after
347 induction of RNAi (green arrows, righthand image for 24 h RNAI in Fig. 8B), there are some
348 flagella that exhibit little if any fluorescence (white arrows). We designate this protein *Tb*EVMP2
349 and suggest that it is a second such protein that is dependent upon *Tb*KH for efficient trafficking
350 to the surface of the flagellum.
351 In contrast, the mNG tagged FLA1 binding protein *Tb*FLA1BP::mNG, which is in the flagellar
352 membrane component of the FAZ (Sun et al., 2013), traffics efficiently to the FM both before and
353 after induction of RNAi (Fig. 8C, 0 h, 24 h, and 48 h RNAi), even in PF parasites that have multiple
354 flagella. Hence, *Tb*FLA1BP does not require *Tb*KH for targeting to the FM, implying that there are
355 both *Tb*KH-dependent and *Tb*KH-independent FM proteins in this parasite.
356

357 **DISCUSSION**

358 In the current study, we have investigated three partners of *Tb*KH: *Tb*KHAP1 and the two
359 related proteins *Tb*KHAP2/MARP1 and *Tb*KHAP3/MARP2. *Tb*KHAP1 can be crosslinked to
360 *Tb*KH by formaldehyde indicating that the two proteins associate within 2-3 Å of each other. The
361 failure to demonstrate crosslinking of *Tb*KHAP2 or *Tb*KHAP3 to *Tb*KH could be due to their more
362 distant location from each other, or to technical difficulties associated with these large highly
363 repetitive proteins, but they are in close enough proximity to give a consistently positive signal
364 using the PLA, that is within ~400 Å. One possibility is that they are part of a multiprotein complex
365 but not in immediate contact with each other. The knockdown of *TbKHAP1* RNA has the most
366 pronounced phenotype, strongly arresting division of BF parasites, inhibiting progression of the
367 cleavage furrow during cytokinesis, and impairing trafficking of *Tb*CaCh/FS179 to the FM. Hence,
368 the phenotypes of RNAi for both *TbKH* and *TbKHAP1* are similar. In contrast, efficient knockdown
369 of *TbKHAP2/3* RNAs slows growth of BF parasites but has a much less severe effect on cell
370 division than knockdown of *TbKHAP1* RNA. In addition, trafficking of *Tb*CaCh/FS179 to the FM
371 is not impaired, even after 7 days of knockdown in BFs. These results imply that although both
372 types of protein likely associate with *Tb*KH in the cytoskeleton, they play different roles. These
373 distinctions in functions could either result from separate complexes between *Tb*KH and each
374 partner or from different roles that each partner plays in the same complex. The association of all
375 partners with the cytoskeleton complicates this issue, as one cannot readily separate different
376 complexes from each other, as would be possible for cytosolic multi-protein complexes.
377 Nonetheless, these studies confirm that *Tb*KH associates with other partner proteins that mediate
378 its activities in different ways.

379 One central activity for *Tb*KH is to traffic *Tb*CaCh/FS179 to the FM, a process that is critical
380 for integrity of the FAZ and for parasite viability. The localization of many PF proteins to their
381 subcellular sites achieved in the TrypTag.org project (Dean et al., 2017) has identified some
382 additional FM proteins, along with some others that were identified previously as FM components
383 from various targeted studies (Kelly et al., 2020a), and one question of relevance is how many of
384 these flagellar surface components rely upon *Tb*KH for organellar trafficking. For *Tb*CaCh/FS179,
385 *Tb*KH appears to be directly involved in trafficking, since the two proteins can be crosslinked by
386 formaldehyde and isolated as molecular partners (Sanchez et al., 2016), but it is possible that
387 others depend upon *Tb*KH either directly or indirectly via the ability of this protein to affect various
388 cellular processes. In this study, we have shown that two FM proteins, *Tb*EVMP1/Fam79.3
389 (Tb927.7.4270) and *Tb*EVMP2 (Tb927.11.1830) are present in both the FM and in EVs secreted
390 from the FM in PF trypanosomes. Both proteins exhibit dependency upon *Tb*KH for trafficking to

391 the FM, as RNAi directed against *TbKH* reduces the efficiency of their localization to this
392 organelle. In contrast, FLA1BP, which participates in adhesion of the flagellum to the cell body by
393 binding to the FLA1 protein in the cell body component of the FAZ (Sun et al., 2013), is not
394 dependent upon *Tb*KH to reach the FM, confirming that both *Tb*KH-dependent and *Tb*KH-
395 independent FM proteins exist.

396 EVs released from the cell body and FM of BF trypanosomes play important roles in virulence
397 of African trypanosomes, including lysis of host erythrocytes leading to anemia, a major
398 mechanism of trypanosome-mediated pathogenesis (Szempruch et al., 2016a; Szempruch et al.,
399 2016b). One might anticipate that surface components of EVs could play important roles in either
400 formation of the EV membrane or interaction of EVs with mammalian or tsetse fly tissues.
401 *TbEVMP1* and *TbEVMP2* mRNAs are both preferentially expressed in PF trypanosomes
402 (tritrypdb.org), but paralogs of *Tb*EVMP1, such as Tb927.7.4230 and Tb927.7.4260, are
403 expressed at higher levels in BFs compared to PFs, suggesting potential roles for such EVMPs
404 in both life cycle stages.

405 The *Tb*KH partners discovered in this study are associated primarily with the subpellicular
406 microtubules, but there are likely to be other partners that may reside principally at the base of
407 the flagellum or in the mitotic spindles and could be associated with distinct activities at those
408 sites. A BioID study by Zhou *et al*. (Zhou et al., 2018) identified five spindle-associated proteins,
409 NuSAP1, NuSAP2, Kif13-1, *Tb*MIP2, and *Tb*AUK1, that are in proximity to *Tb*KH and are thus
410 candidates for molecular partners at the mitotic spindle. In addition, Akiyoshi and Gull (Akiyoshi
411 and Gull, 2014) identified kinetoplast kinetochore proteins (KKTs) that associate with KHARON
412 by CoIP/MS experiments, suggesting a possible role of KHARON in faithful chromosome
413 segregation in kinetoplastid parasites. Molecular interaction studies of the type carried out here
414 will be required to determine which of these proteins may be *bona fide* molecular partners with
415 *Tb*KH and what roles KHARON complexes may be playing at the spindle. Similarly, the ability to
416 isolate flagella with associated kinetoplast DNA and basal bodies (Oberholzer et al., 2011;
417 Robinson and Gull, 1991; Subota et al., 2014) should facilitate identification by either BioID or
418 TAP-MS of *Tb*KH partners at the base of the flagellum. Thus, it should be possible to achieve a
419 comprehensive understanding of the role of KHARON in the cytoskeleton and the distinct
420 functions it carries out in association with different partner proteins.
421

422 **MATERIALS AND METHODS**

423 **Growth and transfection of *T. brucei* cell lines**. BF and PF *T. brucei* cell lines were grown
424 as described previously (Sanchez, 2013). For T7 RNA polymerase-independent expression, the
425 BF/pHD1313 or PF/pHD1313 clones were employed (Sanchez et al., 2016). For T7 RNA
426 polymerase driven expression in BF, *T. brucei* 427 parasites transfected with the pSmOx (Poon
427 et al., 2012) plasmid expressing the tetracycline repressor and T7 RNA polymerase were
428 generated and grown in 0.1 µg/ml puromycin. For T7 RNA polymerase driven expression in PF,
429 *T. brucei* 427 13-6 clone expressing TETR and T7 RNA polymerase was used (Wirtz et al., 1999).
430 Linear plasmid or PCR DNA amplicons were used to transfect mid-log phase parasites as
431 described (Sanchez et al., 2016). Transfected clones were obtained by limiting dilution according
432 to published protocols (Burkard et al., 2007; McCulloch et al., 2004) .

433 **Primary amino acid sequence analysis**. For DNA and amino acid sequence analysis of
434 *TbKHAPs*, ExPASy, via the SIB Bioinformatics Resource Portal (http://expasy.org), and
435 GeneBank (http://blast.ncbi.nlm.nih.gov/Blast.cgi) or TritrypDB (http://tritrypdb.org/tritrypdb) were
436 used.

437 **Inhibition of gene expression by RNAi**. To inhibit the expression of *Tb*KH, *Tb*KHAPs or
438 *Tb*FLA1, a number of cell lines were generated employing different genetic backgrounds. The BF
439 and PF TbKH^{RNAi} and *Tb*FLA1^{RNAi} clones, for which expression is T7 polymerase-independent,
440 were previously described (Sanchez et al., 2016), and RNAi was induced by adding doxycycline
441 (1 µg/ml) to the culture medium. The BF and PF *Tb*KHAP1^{RNAi} clones were generated by
442 subcloning the first 500 bp of the *TbKHAP1* (Tb927.10.1026) ORF into the pZJM RNAi vector,
443 where expression is driven by two opposing T7 promoters (Wang et al., 2000). Similarly, BF and
444 PF TbKHAP2/3^{RNAi} clones were generated by subcloning the last 500 bp of *TbKHAP2*
445 (Tb927.10.10360) that is almost identical to the *TbKHAP3* (Tb927.10.10280) ORF into the pZJM
446 RNAi vector. RNAi clones were selected by resistance to 2.5 µg/ml phleomycin and 0.1 µg/ml
447 puromycin, and expression of dsRNA was induced by addition of 1 µg/ml doxycycline. To verify
448 inhibition of *Tb*KHAP1-3 expression, total cell lysates were obtained from parasite cultures
449 induced for RNAi and subjected to Western blot experiments as indicated below.

450 **Endogenous epitope tagging**. For endogenous tagging of *Tb*KH, *Tb*KHAP1, *Tb*KHAP2,
451 *Tb*KHAP3, CAP-15, *Tb*CaCh (FS179), *Tb*EVMP1, *Tb*EVMP2 and *Tb*FLA1BP at the N-terminus
452 or C-terminus, different epitopes were employed as indicated in the text, following the protocol
453 described (Dean et al., 2015). Briefly, epitope-tagging cassettes were generated by using two
454 specific 100 nt oligonucleotides containing ~80 nt each that are homologous to the ORF region
455 to be tagged and ~20 nt homologs to the plasmid pPOTV4 template flanking the drug resistance

456 marker cassette, and using the universal PCR settings. Epitope tagging PCR cassettes were
457 ethanol precipitated and resuspended in 10 µl of nucleofection buffer (Wang et al., 2000), then
458 parasites were transfected with the purified tagging cassettes as described (Dean et al., 2015)
459 and selected using 1.5 µg/ml G418 (15 µg ml^{-1} for PF) or 0.1 µg/ml puromycin (1 µg/ml for PF),
460 and cloned by limiting dilution.

461 **Generation of Rabbit anti-*Tb*KH antibody**. A custom rabbit anti-*Tb*KH polyclonal antibody
462 (pAb) was generated by GenScript, using their 49-day antibody generation protocol. Briefly, two
463 rabbits were injected with 200 µg of His_6::*Tb*KH, representing amino acids 43 - 411, emulsified in
464 Freund's complete adjuvant. The rabbit was boosted 3 times at 14-day intervals with 200 µg of
465 His_6::*Tb*KH emulsified in Freund's incomplete adjuvant. Antibody specificity for *Tb*KH was
466 evaluated by Western blot comparing the reactivities of the rabbit serum from immunized rabbits
467 to *T. brucei* protein lysates from wild-type cells and N-BirA*::*Tb*KH cell line (Fig 3A). Proteins were
468 immunodetected using 1:2500 dilution of the rabbit anti-*Tb*KH polyclonal antibody and 1:15,000
469 dilution of goat anti-rabbit-HRP antibody (Sigma-Aldrich). The chemiluminescent protocol was
470 used for developing as indicated below.

471 **Immunofluorescence microscopy**. For immunofluorescence microscopy, 5 X 10^6 parasites
472 were centrifuged at 1000 X g for 5 min and washed twice at room temperature with phosphate
473 buffered saline pH 7.2 (PBS) containing 10 mM glucose. The cell pellet was resuspended in 4%
474 paraformaldehyde in PBS, pH 7.2 and incubated for 15 min at room temperature, cells were
475 centrifuged as descried above and washed once with PBS, resuspended in 100 µl PBS, spotted
476 onto poly-L-lysine coated coverslips, and blocked with 2% goat serum, 0.01 sodium azide, 0.01
477 saponin in PBS (blocking solution) for 1 h at room temperature, rinsed 3 X with PBS, and
478 incubated with primary antibodies for 1 h at room temperature. The following primary antibodies
479 were employed: 1:250 dilution rabbit anti-*Tb*KH pAb (reported in this work), 1:500 dilution mouse
480 anti-HA monoclonal antibody (mAb) (BioLegend, Cat # MMS-101R), and 1:1000 dilution mouse
481 anti-α-tubulin mAb (Sigma-Aldrich, Cat. # T5168). Subsequently, cells were rinsed as before and
482 incubated with a 1:1000 dilution of secondary antibodies coupled to Alexa Fluor dyes (Molecular
483 Probes) as follows: Alexa Fluor® 488 goat anti-mouse IgG (H+L) (Cat. # A11001), Alexa Fluor®
484 594 goat anti-mouse IgG (H+L) (Cat. # A11005), Alexa Fluor® 594 goat anti-rabbit IgG (H+L)
485 (Cat. # A11012) and Alexa Fluor® 488 goat anti-rabbit IgG (H+L) (Cat. # A11008), as indicated,
486 in blocking solution for 1h at room temperature in the dark. Cover slips were rinsed 3 X with PBS
487 and mounted onto slides using DAPI Fluoromount-G (SouthernBiotech). Fluorescence images
488 were obtained using a wide field deconvolution system (Applied Precision Instruments, Inc.)
489 consisting of an inverted Nikon TE 200 Eclipse microscope, a Kodak CH350 CCD camera, and

490 the Deltavision operating system. Images were acquired using a 60 X objective and 1.25 X
491 magnification in a 1024 X 1024 format, and deconvolved using SoftWoRx software. Adobe
492 Photoshop CC and Adobe Illustrator CC (Adobe Systems Inc.) were used to create image
493 compositions.

494 **Flagellar protein purification, formaldehyde crosslinking, pull down, and Western blot**
495 **assay**. Flagellar purification was performed as described (Subota et al., 2014) with slight
496 changes. Briefly, BF or PF *Tb*KH1^{RNAi}, *Tb*FLA1^{RNAi}, *Tb*KHAP1^{RNAi} and *Tb*KHAP2/3^{RNAi} clones were
497 grown in 1 µg/ml doxycycline for the indicated times and pelleted at 420 X g for 10 min. Cell pellets
498 were washed with buffer A (25 mM Na^+-tricine, pH 7, 1% BSA, 0.1 mM $CaCl_2$, 0.2 mM EDTA, 5
499 mM $MgCl_2$ and 12 mM β-mercaptoethanol) containing 0.32 M sucrose and centrifuged at 420 X g
500 for 10 min. Cell pellets were gently resuspended at 3 X 10^8 parasites/ml in buffer A plus 0.3 M
501 sucrose, transferred into Eppendorf tubes and vortexed for 5 min or until microscopic verification
502 of flagellum detachment, followed by centrifugation at 420 X g for 10 min. Supernatants were
503 recovered and centrifuged at 16,000 X g for 20 min at 4 °C. Pellets containing the isolated flagella
504 were resuspended in 200 µl of PBS and used for immunofluorescence microscopy. Also,
505 purification of flagellar cytoskeletons from BF or PF clones was performed by isolation of whole
506 cytoskeletons followed by treatment with 1 mM $CaCl_2$ to solubilize the pellicular cytoskeletons,
507 according to Imhof et al. (Imhof et al., 2019).

508 For formaldehyde crosslinking and pull down, cell lines were prepared that expressed *Tb*KH1
509 endogenously tagged with the His_{10} epitope at the N-terminus (His_{10}::*Tb*KH1) and also co-
510 expressed with a protein of interest endogenously tagged at its N- or C-terminus with a HA_3 or
511 $V5_3$ epitope (HA_3::*Tb*KHAP1, HA_3::*Tb*KHAP2, *Tb*KHAP2::HA_3, $V5_3$::*Tb*KHAP3, HA_3::*Tb*KHAP3
512 and *Tb*CAP15::HA_3). Parasites were washed once with PBS and pelleted at 1000 X g for 10 min,
513 and cell pellets resuspended in 9.37 ml PBS plus 0.63 ml 16% formaldehyde-EM grade
514 (Polysciences, Inc) and incubated at room temperature for 10 min. For non-crosslinked control
515 samples, PBS was added instead of formaldehyde. Subsequently, 1 ml of 2.5 M glycine in PBS
516 was added to the crosslinked samples and incubated at room temperature for 5 min, crosslinked
517 parasites were pelleted at 1000 X g for 10 min and washed twice with PBS. Then, cell pellets with
518 or without crosslinking were resuspended in 1 ml of Buffer 1 (8 M urea, 300 mM NaCl, 0.5%
519 Nonidet P-40, 50 mM NaH_2PO_4, 50 mM Tris, pH 7.0) on ice. Samples were sonicated 3 times on
520 ice at 50% max amplitude (Sonic Dismembrator, 500W, Fisher Scientific) for 10 s with 30 s
521 between pulses. A 2.5% aliquot of this protein lysate was saved as the protein lysate fraction (LF).

522 The remainder of the protein was incubated with 750 µl of HisPur™ Cobalt Resin (Thermo
523 Scientific Pierce, Rockford, IL) on a rocker for 45 min at room temperature. The resins were

524 washed 5 times with 1 ml of Buffer 1 (5 min each), 5 times with 1 ml of Buffer 1 at pH 6.4 (5 min
525 each), and 5 times with 1 ml of Buffer 1 pH 6.4 plus 10 mM imidazole (5 min each). Cobalt bound
526 protein complexes were eluted with 1 ml of Buffer 2 (45 mM NaH_2PO_4, 8 M urea, 270 mM NaCl,
527 150 mM imidazole). Eluate fractions (EF) were concentrated using Amicon Ultra-0.5 Centrifugal
528 Filter Units, 10K NMWL (Millipore Sigma). Crosslinking was reversed by boiling protein samples
529 for 30 min in 1X Bolt™-LDS sample buffer containing 10 mM DTT.
530 Protein extracts were prepared and analyzed by Western blot employing Bolt™ 4-12% Bis-Tris
531 Mini Protein Gels or NuPage™ 3-8% Tris-acetate gels, Mini Gel Tank and Mini Blot Module
532 following the manufacturer's instructions (Life Technologies). Proteins were transferred onto
533 PVDF membranes (Millipore). Protein immunodetection was done using rabbit anti-*Tb*KH pAb at
534 1:2500 dilution, mouse anti-HA mAb (BioLegend, Cat # MMS-101R) 1:2500 dilution, mouse anti-
535 V5 mAb (Invitrogen, Cat # MA5-15253) 1:2500 dilution, and mouse anti-α tubulin mAb (Sigma-
536 Aldrich, Cat. # T5168) 1:10,000 dilution. Goat anti-rabbit-HRP (Sigma-Aldrich) 1:15,000 dilution
537 and goat anti-mouse-HRP (Jackson ImmunoResearch Laboratories, Cat. # 115-03-174, Lot #
538 117119) were used as secondary antibodies and Western blots were developed using the
539 SuperSignal™ West Pico Plus Chemiluminescent Substrate (Thermo Fisher Scientific) and an
540 Image Quant LAS 400 (GE Healthcare) scanner was employed to acquire luminescent images.
541 Adobe Photoshop CC and Adobe Illustrator CC (Adobe Systems Inc.) were used to create image
542 compositions.
543 **Proximity ligation assay (PLA)**. Mid-log BF or PF parasites were harvested by
544 centrifugation at 1000 x g for 10 min, washed once in PBS and fixed with 4% paraformaldehyde
545 in PBS for 15 min at room temperature. Fixed cells were attached to cover slips and
546 permeabilized as indicated above for immunofluorescence analysis. Subsequently the PLA
547 protocol was followed according to the Duolink In Situ Red Starter Kit Mouse/Rabbit (Millipore
548 Sigma) instructions. Briefly, after blocking cells were incubated with 1:250 dilution of rabbit anti-
549 *Tb*KH pAb and 1:500 dilution of mouse anti-HA mAb (BioLegend, Cat# MMS-101R). As a
550 negative control, cells were incubated only with 1:250 dilution of the rabbit anti-*Tb*KH pAb. Then
551 PLA species-specific secondary antibodies with minus and plus oligonucleotide probes were
552 added, followed by ligation, amplification and hybridization with specific red-fluorescent
553 oligonucleotides to allow detection by fluorescence microscopy. Samples were mounted and
554 imaged as described for immunofluorescence analysis.
555
556 **Acknowledgements**
557 We appreciate the expert advice and support of the staff of the Advanced Light Microscopy

558 Core in the Jungers Center for Neurosciences at Oregon Health & Science University. We
559 acknowledge discussions with Dr. Samuel Dean (University of Oxford) concerning new flagellar
560 membrane proteins identified by the TrypTag project.
561

562 **Competing interests**

563 The authors declare no competing or financial interests.
564

565 **Author contributions**

566 Conceptualization: M.A.S. and S.M.L.; Data collection: M.A.S.; Data analysis: M.A.S. and
567 S.M.L.; Writing and editing: M.A.S. and S.M.L.; Funding acquisition and project administration:
568 S.M.L.
569

570 **Funding**

571 This work was supported by National Institutes of Health grant AI121160 to S.M.L. The content is
572 solely the responsibility of the authors and does not necessarily represent the official views of the
573 National Institutes of Health.
574

575 **References**

576 **Affolter, M., Hemphill, A., Roditi, I., Muller, N. and Seebeck, T.** (1994). The repetitive
577 microtubule-associated proteins MARP-1 and MARP-2 of *Trypanosoma brucei*. *J Struct Biol* **112**,
578 241-51.

579 **Akiyoshi, B. and Gull, K.** (2014). Discovery of unconventional kinetochores in
580 kinetoplastids. *Cell* **156**, 1247-1258.

581 **Baudieri, B. and Tomassini, N.** (1962). Fine struttura dei tripanosomi. *Parassitologia* **4**,
582 89-95.

583 **Burkard, G., Fragoso, C. M. and Roditi, I.** (2007). Highly efficient stable transformation
584 of bloodstream forms of *Trypanosoma brucei*. *Mol Biochem Parasitol* **153**, 220-3.

585 **Cayla, M., Rojas, F., Silvester, E., Venter, F. and Matthews, K. R.** (2019). African
586 trypanosomes. *Parasit Vectors* **12**, 190.

587 **Dang, H. Q., Zhou, Q., Rowlett, V. W., Hu, H., Lee, K. J., Margolin, W. and Li, Z.** (2017).
588 Proximity Interactions among basal body components in *Trypanosoma brucei* identify novel
589 regulators of basal body biogenesis and inheritance. *mBio* **8**.

590 **Dean, S., Sunter, J., Wheeler, R. J., Hodkinson, I., Gluenz, E. and Gull, K.** (2015). A
591 toolkit enabling efficient, scalable and reproducible gene tagging in trypanosomatids. *Open Biol*
592 **5**, 140197.

593 **Dean, S., Sunter, J. D. and Wheeler, R. J.** (2017). TrypTag.org: A trypanosome genome-
594 wide protein localisation resource. *Trends Parasitol* **33**, 80-82.

595 **Ellis, D. S., Ormerod, W. E. and Lumsden, W. H. R.** (1976). Filaments of "*Trypanosoma*
596 *brucei*": some notes on differences in origin and structure in two stains of "*Trypanosoma*
597 *(Trypanozoon) brucei rhodesiense*". *Acta Tropica* **33**, 151-168.

598 **Farr, H. and Gull, K.** (2012). Cytokinesis in trypanosomes. *Cytoskeleton (Hoboken)* **69**,
599 931-41.

600 **Fredriksson, S., Gullberg, M., Jarvius, J., Olsson, C., Pietras, K., Gustafsdottir, S.**
601 **M., Ostman, A. and Landegren, U.** (2002). Protein detection using proximity-dependent DNA
602 ligation assays. *Nat Biotechnol* **20**, 473-7.

603 **Hemphill, A., Affolter, M. and Seebeck, T.** (1992). A novel microtubule-binding motif
604 identified in a high molecular weight microtubule-associated protein from *Trypanosoma brucei*. *J*
605 *Cell Biol* **117**, 95-103.

606 **Hoffman, E. A., Frey, B. L., Smith, L. M. and Auble, D. T.** (2015). Formaldehyde
607 crosslinking: a tool for the study of chromatin complexes. *J Biol Chem* **290**, 26404-11.

608 **Imhof, S., Zhang, J., Wang, H., Bui, K. H., Nguyen, H., Atanasov, I., Hui, W. H., Yang,**
609 **S. K., Zhou, Z. H. and Hill, K. L.** (2019). Cryo electron tomography with Volta phase plate reveals
610 novel structural foundations of the 96-nm axonemal repeat in the pathogen *Trypanosoma brucei*.
611 *Elife* **8**.
612 **Ishida, T. and Kinoshita, K.** (2007). PrDOS: prediction of disordered protein regions from
613 amino acid sequence. *Nucleic Acids Res* **35**, W460-4.
614 **Kaiser, P., Meierhofer, D., Wang, X. and Huang, L.** (2008). Tandem affinity purification
615 combined with mass spectrometry to identify components of protein complexes. *Methods Mol Biol*
616 **439**, 309-26.
617 **Kelly, F. D., Sanchez, M. A. and Landfear, S. M.** (2020a). Touching the surface: Diverse
618 roles for the flagellar membrane in Kinetoplastid parasites. *Microbiol Mol Biol Rev* **84**, e00079-19.
619 **Kelly, F. D., Tran, K. D., Hatfield, J., Schmidt, K., Sanchez, M. A. and Landfear, S. M.**
620 (2020b). A cytoskeletal protein complex is essential for division of intracellular amastigotes of
621 *Leishmania mexicana*. *J Biol Chem* **295**, 13106-13122.
622 **Kennedy, P. G.** (2013). Clinical features, diagnosis, and treatment of human African
623 trypanosomiasis (sleeping sickness). *Lancet Neurol* **12**, 186-94.
624 **Langousis, G. and Hill, K. L.** (2014). Motility and more: the flagellum of *Trypanosoma*
625 *brucei*. *Nat Rev Microbiol* **12**, 505-18.
626 **MacLean, L., Myburgh, E., Rodgers, J. and Price, H. P.** (2013). Imaging African
627 trypanosomes. *Parasite Immunol* **35**, 283-94.
628 **Manna, P. T., Boehm, C., Leung, K. F., Natesan, S. K. and Field, M. C.** (2014). Life and
629 times: synthesis, trafficking, and evolution of VSG. *Trends Parasitol* **30**, 251-8.
630 **McCulloch, R., Vassella, E., Burton, P., Boshart, M. and Barry, J. D.** (2004).
631 Transformation of monomorphic and pleomorphic *Trypanosoma brucei*. *Methods Mol Biol* **262**,
632 53-86.
633 **McGuffin, L. J., Bryson, K. and Jones, D. T.** (2000). The PSIPRED protein structure
634 prediction server. *Bioinformatics* **16**, 404-5.
635 **Mitchell, A., Chang, H. Y., Daugherty, L., Fraser, M., Hunter, S., Lopez, R., McAnulla,**
636 **C., McMenamin, C., Nuka, G., Pesseat, S. et al.** (2015). The InterPro protein families database:
637 the classification resource after 15 years. *Nucleic Acids Res* **43**, D213-21.
638 **Molloy, J. O. and Ormerod, W. E.** (1964). A fibril emerging from the posterior end of
639 *Trypanosoma rhodesiense*. *Philos Trans R Soc Lond B Biol Sci* **58**, 2.
640 **Oberholzer, M., Langousis, G., Nguyen, H. T., Saada, E. A., Shimogawa, M. M.,**
641 **Jonsson, Z. O., Nguyen, S. M., Wohlschlegel, J. A. and Hill, K. L.** (2011). Independent analysis

642 of the flagellum surface and matrix proteomes provides insight into flagellum signaling in
643 mammalian-infectious *Trypanosoma brucei*. *Mol Cell Proteomics* **10**, M111 010538.
644 **Poon, S. K., Peacock, L., Gibson, W., Gull, K. and Kelly, S.** (2012). A modular and
645 optimized single marker system for generating *Trypanosoma brucei* cell lines expressing T7 RNA
646 polymerase and the tetracycline repressor. *Open Biol* **2**, 110037.
647 **Robinson, D. R. and Gull, K.** (1991). Basal body movements as a mechanism for
648 mitochondrial genome segregation in the trypanosome cell cycle. *Nature* **352**, 731-3.
649 **Roux, K. J., Kim, D. I., Raida, M. and Burke, B.** (2012). A promiscuous biotin ligase
650 fusion protein identifies proximal and interacting proteins in mammalian cells. *J Cell Biol* **196**, 801-
651 10.
652 **Sanchez, M. A.** (2013). Molecular identification and characterization of an essential
653 pyruvate transporter from *Trypanosoma brucei*. *J Biol Chem* **288**, 14428-37.
654 **Sanchez, M. A., Tran, K. D., Valli, J., Hobbs, S., Johnson, E., Gluenz, E. and Landfear,**
655 **S. M.** (2016). KHARON Is an essential cytoskeletal protein involved in the trafficking of fagellar
656 membrane proteins and cell division in African trypanosomes. *J Biol Chem* **291**, 19760-73.
657 **Santi, A. M. M., Lanza, J. S., Tunes, L. G., Fiuza, J. A., Roy, G., Orfano, A. D. S., de**
658 **Carvalho, A. T., Frezard, F., Barros, A. L. B., Murta, S. M. F. et al.** (2018). Growth arrested
659 live-attenuated *Leishmania infantum* KHARON1 null mutants display cytokinesis defect and
660 protective immunity in mice. *Sci Rep* **8**, 11627.
661 **Schepilewsky, E.** (1912). Fadenförmige anhängsel bei den trypanosomen. *Zbl. Bakt.* **65**,
662 79-83.
663 **Schneider, A., Hemphill, A., Wyler, T. and Seebeck, T.** (1988). Large microtubule-
664 associated protein of *T. brucei* has tandemly repeated, near-identical sequences. *Science* **241**,
665 459-62.
666 **Shimogawa, M. M., Saada, E. A., Vashisht, A. A., Barshop, W. D., Wohlschlegel, J.**
667 **A. and Hill, K. L.** (2015). Cell surface proteomics provides insight into stage-specific remodeling
668 of the host-parasite interface in *Trypanosoma brucei*. *Mol Cell Proteomics* **14**, 1977-88.
669 **Soderberg, O., Gullberg, M., Jarvius, M., Ridderstrale, K., Leuchowius, K. J., Jarvius,**
670 **J., Wester, K., Hydbring, P., Bahram, F., Larsson, L. G. et al.** (2006). Direct observation of
671 individual endogenous protein complexes *in situ* by proximity ligation. *Nat Methods* **3**, 995-1000.
672 **Sonnhammer, E. L., Eddy, S. R., Birney, E., Bateman, A. and Durbin, R.** (1998). Pfam:
673 multiple sequence alignments and HMM-profiles of protein domains. *Nucleic Acids Res* **26**, 320-
674 2.

675 **Subota, I., Julkowska, D., Vincensini, L., Reeg, N., Buisson, J., Blisnick, T., Huet, D.,**
676 **Perrot, S., Santi-Rocca, J., Duchateau, M. et al.** (2014). Proteomic analysis of intact flagella of
677 procyclic *Trypanosoma brucei* cells identifies novel flagellar proteins with unique sub-localization
678 and dynamics. *Mol Cell Proteomics* **13**, 1769-86.
679 **Sun, S. Y., Wang, C., Yuan, Y. A. and He, C. Y.** (2013). An intracellular membrane
680 junction consisting of flagellum adhesion glycoproteins links flagellum biogenesis to cell
681 morphogenesis in *Trypanosoma brucei*. *J Cell Sci* **126**, 520-31.
682 **Szempruch, A. J., Dennison, L., Kieft, R., Harrington, J. M. and Hajduk, S. L.** (2016a).
683 Sending a message: extracellular vesicles of pathogenic protozoan parasites. *Nat Rev Microbiol*
684 **14**, 669-675.
685 **Szempruch, A. J., Sykes, S. E., Kieft, R., Dennison, L., Becker, A. C., Gartrell, A.,**
686 **Martin, W. J., Nakayasu, E. S., Almeida, I. C., Hajduk, S. L. et al.** (2016b). Extracellular vesicles
687 from *Trypanosoma brucei* mediate virulence factor transfer and cause host anemia. *Cell* **164**,
688 246-257.
689 **Tran, K. D., Rodriguez-Contreras, D., Vieira, D. P., Yates, P. A., David, L., Beatty, W.,**
690 **Elferich, J. and Landfear, S. M.** (2013). KHARON1 mediates flagellar targeting of a glucose
691 transporter in *Leishmania mexicana* and is critical for viability of infectious intracellular
692 amastigotes. *J. Biol. Chem.* **288**, 22721-22733.
693 **Tran, K. D., Vieira, D. P., Sanchez, M. A., Valli, J., Gluenz, E. and Landfear, S. M.**
694 (2015). *Kharon1* null mutants of *Leishmania mexicana* are avirulent in mice and exhibit a
695 cytokinesis defect within macrophages. *PLoS One* **10**, e0134432.
696 **Uversky, V. N.** (2013). The alphabet of intrinsic disorder: II. Various roles of glutamic acid
697 in ordered and intrinsically disordered proteins. *Intrinsically Disord Proteins* **1**, e24684.
698 **Vaughan, S. and Gull, K.** (2008). The structural mechanics of cell division in
699 *Trypanosoma brucei*. *Biochem Soc Trans* **36**, 421-4.
700 **Vedrenne, C., Giroud, C., Robinson, D. R., Besteiro, S., Bosc, C., Bringaud, F. and**
701 **Baltz, T.** (2002). Two related subpellicular cytoskeleton-associated proteins in *Trypanosoma*
702 *brucei* stabilize microtubules. *Mol Biol Cell* **13**, 1058-70.
703 **Vickerman, K. and Luckins, A. G.** (1969). Localization of variable antigens in the surface
704 coat of *Trypanosoma brucei* using ferritin conjugated antibody. *Nature* **224**, 1125-1126.
705 **Wang, Z., Morris, J. C., Drew, M. E. and Englund, P. T.** (2000). Inhibition of
706 *Trypanosoma brucei* gene expression by RNA interference using an integratable vector with
707 opposing T7 promoters. *J Biol Chem* **275**, 40174-9.

708 **Wheeler, R. J., Gull, K. and Sunter, J. D.** (2019). Coordination of the Cell Cycle in
709 Trypanosomes. *Annu Rev Microbiol* **73**, 133-154.
710 **Wirtz, E., Leal, S., Ochatt, C. and Cross, G. A. M.** (1999). A tightly regulated inducible
711 expression system for conditional gene knock-outs and dominant-negative genetics in
712 *Trypanosoma brucei*. *Mol. Biochem. Parasitol.* **99**, 89-101.
713 **Wright, K. A. and Lumsden, W. H. R.** (1970). The formation of filopodium-like processes
714 by *Trypanosoma*. *J. Cell Sci.* **6**, 285-297.
715 **Zhang, T., Faraggi, E., Li, Z. and Zhou, Y.** (2013). Intrinsically semi-disordered state and
716 its role in induced folding and protein aggregation. *Cell Biochem Biophys* **67**, 1193-205.
717 **Zhou, Q., Lee, K. J., Kurasawa, Y., Hu, H., An, T. and Li, Z.** (2018). Faithful chromosome
718 segregation in *Trypanosoma bruce*i requires a cohort of divergent spindle-associated proteins
719 with distinct functions. *Nucleic Acids Res* **46**, 8216-8231.
720
721

722 **FIGURE LEGENDS**

723 **Fig. 1. *Tb*KH localizes in three distinct subcellular compartments.** (A) Flagellar preparation
724 from *Tb*FLA1^{RNAi} cell line, isolated after 72 h of induction with 1 µg/ml doxycycline (dox), stained
725 with DAPI (*blue*) and immunostained with anti-*Tb*KH pAb (*Tb*KH, *red*). *Tb*KH localization at the
726 base of the flagellum is indicated by the *red arrowhead*. (B) Wild type BF parasites were
727 immunostained with anti-*Tb*KH pAb (*Tb*KH, *red*) and stained with DAPI. These images display a
728 parasite in which *Tb*KH staining is associated with both the subpellicular microtubules (*right*
729 *arrowheads*) and the mitotic spindle that connects the two nuclei late during mitosis (*left*
730 *arrowheads*). DIC indicates images collected by differential interference contrast microscopy.
731 (C) Western blot of total protein lysates from BF trypanosomes that are either wild type (*WT*) or
732 expressing BirA*::TbKH fusion protein (*A**). Blot was probed with anti-*Tb*KH pAb and developed
733 by chemiluminescence. Specific immunodetected proteins corresponding to the native *Tb*KH
734 and the BirA*::*Tb*KH fusion protein are shown. Relative protein molecular weights are shown in
735 kDa, as determined by mobility relative to molecular weight markers.

736 **Fig. 2. Subcellular localization of *Tb*KHAPs in BF and PF *T. brucei*.** (A, B) The HA_3::TbKHAP1
737 cell line was immunostained with anti-HA mAb (HA_3::*Tb*KHAP1*, green*) and anti-*Tb*KH pAb
738 (*Tb*KH*, red*). (C, D) The TbKHAP2::HA_3 cell line was stained with anti-HA mAb (*Tb*KHAP2::HA_3*,*
739 *green*) and anti-*Tb*KH pAb (*Tb*KH*, red*). (E) The BF 3V5::*Tb*KHAP3 and (F) PF HA_3::*Tb*KHAP3
740 cell lines were immunostained with (E) anti-V5 mAb (3V5::*Tb*KHAP3, *green)* or (F) anti-HA mAb
741 (HA_3::*Tb*KHAP3*, green*) and anti-*Tb*KH pAb (*Tb*KH*, red*). All preparations were stained with DAPI,
742 which detects both nuclear and kinetoplast DNA (*blue*). DIC images were also acquired from all
743 samples.

744 **Fig. 3. KHARON and KHAPs colocalize at the base of the flagellum in *T. brucei.*** (A) Whole
745 isolated flagella from the BF HA_3::*Tb*KHAP1/*Tb*FLA1^{RNAi} clone induced for RNAi for 72 h, were
746 immunostained with anti-HA mAb (HA_3::*Tb*KHAP1, *green*) and anti-*Tb*KH pAb (*Tb*KH, *red*) and
747 stained with DAPI (*blue*). (A, left panel) shows an immunofluorescence/DIC image of an isolated
748 flagellum, *black punctuated* box indicates the magnified area depicted in (A, center-right, center-
749 left and left) panels. *Green arrowheads* indicate HA_3::*Tb*KHAP1 localization, *red arrowheads*
750 indicate *Tb*KH localization and *yellow arrowheads* indicate overlapping signals, when channels
751 are merged, near the kinetoplast (*blue*). (B) Flagellar cytoskeletons were isolated from BF
752 trypanosomes expressing HA_3::TbKHAP2 and imaged as described in (A). (C) Flagellar
753 cytoskeletons were isolated from PF trypanosomes expressing HA_3::TbKHAP3 and imaged as
754 described in (A).

755 **Fig. 4. *Tb*KH is closely associated with *Tb*KHAP1, *Tb*KHAP2, and *Tb*KHAP3.** (A) Western
756 blot of protein samples from pull down of HA_3::*Tb*KHAP1 using His_{10}::*Tb*KH as a bait and
757 CAP15::HA_3 as negative control. *LS* and *EF*, lysate and elution fractions without formaldehyde
758 crosslinking; *LS** and *EF**, lysate and elution fraction with formaldehyde crosslinking. Protein blots
759 were developed by chemiluminescence, bands are indicated by protein names, and migration of
760 molecular weight markers are designated in kDa. (B, C) PLA employing BF or PF
761 HA_3::TbKHAP1/His_{10}::TbKH cell lines, as indicated. For these and all subsequent sections of this
762 figure, the *left panel* shows results using both anti-HA mAb and anti-*Tb*KH pAb, and the *right*
763 *panel* shows results using only the anti-*Tb*KH pAb, as the negative control. *Red puncta* indicate
764 positive HA_3::*Tb*KHAP1-*Tb*KH interaction. DIC images were acquired from all samples.
765 (D, E) PLA employing BF or PF *Tb*KHAP2::HA_3 cell lines, as indicated. *Red puncta* indicate
766 positive *Tb*KHAP2-*Tb*KH interaction. (F, G*)* PLA employing BF or PF HA_3::*Tb*KHAP3 cell lines,
767 as indicated using. *Red puncta* indicate positive *Tb*KHAP3-*Tb*KH interaction.
768 **Figure 5. Depletion of *Tb*KHAP1 is lethal for *T. brucei* parasites.** (A) Western blot of total
769 protein lysates from TbKHAP1^{RNAi} BF parasites grown in the presence of doxycycline (+dox)
770 and immunodetected with anti-HA mAb, anti-*Tb*KH pAb. The approximate molecular weights in
771 kDa of HA_3::*Tb*KHAP1 and *Tb*KH are indicated as determined by mobility compared to weight
772 markers. *Numbers* under the blot represent the relative intensity (*RI*) of HA_3::*Tb*KHAP1 protein
773 normalized to the *Tb*KH protein level. (B) Cell density for induced (*empty circles*) and non-
774 induced (*filled circles*) *Tb*KHAP1^{RNAi} BF cell lines. Parasite density was quantified by phase
775 contrast microscopy using a hemocytometer. Data represent the averages and standard
776 deviations of two experiments, each employing an independently isolated *Tb*KHAP1^{RNAi} clonal
777 cell line, and technical replicates were also performed for each biological replicate. Standard
778 deviations are too small to be visible. (C) Microscopic analysis of nuclei and kinetoplast
779 numbers of BF *Tb*KHAP1^{RNAi} parasites following induction of RNAi. Data represent frequency
780 (*%*) of cells with different numbers of DAPI stained nuclei (*N*) and kinetoplasts (*K*). Results
781 represent the average and range of two independent experiments. Brackets compare 0 h to 48
782 h doxycycline induction, with *** representing $P<0.001$, as determined by 2-way ANOVA using
783 Dunnett's multiple comparison test, where all time points were compared to 0 h doxycycline but
784 only statistical significance for 48 h is shown. (D-F) *Tb*KHAP1^{RNAi} BF parasites were stained
785 with DAPI (*blue*) and immunostained with anti-α-tubulin mAb (Tub, *red*) at (D) 0 h, (E) 20 h and
786 (F) 48 h post-RNAi induction. In (E) the *white arrowhead* indicates a cell with a tadpole-like
787 morphology and the *yellow arrowhead* indicates a cell with two flagella at opposite poles of the
788 cell body.

789 **Fig. 6. Phenotypes resulting from RNAi directed against *TbKHAP2* and *TbKHAP3*.** (*A*)
790 Western blot of total protein lysates of BF parasites expressing $HA_{3::}$*Tb*KHAP2 following
791 induction of RNAi (1 µg ml^{-1} doxycycline, *dox*) directed against *TbKHAP2/3* RNAs. Protein blots
792 were probed with anti-HA mAb and anti-*Tb*KH pAb as loading control. Molecular weight markers
793 are indicated in kDa. (*B*) Growth curve of induced (*empty circles*) and non-induced (*filled circles*)
794 TbKHAP2/3^{RNAi} cell line. Parasite density was quantified by phase contrast microscopy using a
795 hemocytometer. The data represent two biological replicate experiments, but the standard
796 deviations are too small to see in the figure. Representative *Tb*KHAP2/3^{RNAi} cells induced for
797 RNAi were stained with DAPI (*blue*) and immunostained with anti-*Tb*KH pAb (*Tb*KH, *red*) at (*C)*
798 0 h and (*D)* 4 days post-RNAi induction. *White arrowhead* in (*D*) indicates a cell showing
799 aberrant morphology. DIC images were obtained for all samples. (*E*) Microscopic analysis of NK
800 in BF parasites induced for RNAi. Frequency (*%*) of cells with different numbers of nuclei (*N*)
801 and kinetoplasts (*K*) at different times following induction of RNAi against *TbKHAP2/3* mRNA.
802 Results represent the average and range of two independent experiments. Statistical
803 comparisons were performed as in Fig. 5C, with *** representing P<0.001, ** P<0.01, and *
804 P<0.05.
805 **Fig. 7. Knockdown of *Tb*KHAP1, but not *Tb*KHAP2 or *Tb*KHAP3, impairs trafficking of**
806 ***Tb*CaCh::HA_3 to the flagellum.** (A-C)*Tb*CaCh::HA_3/*Tb*KHAP1^{RNAi} BF cell line was induced with
807 1 µg/ml doxycycline (dox). Parasites were stained with DAPI (*blue*) and immunostained with
808 anti-HA mAb (*Tb*CaCh::HA_3*, green*) and anti-*Tb*KH pAb (*Tb*KH*, red*). (A) Non-induced
809 TbCaCh::HA_3/TbKHAP1^{RNAi} parasites (*0 h dox*), (B) parasites induced for 24 h (2*4 h dox*) and
810 (C*)* parasites induced for 48 h (*48 h dox*). *Green arrowheads* in (A-C) indicate flagella where
811 *Tb*CaCh::HA_3 is present, and *white arrowheads* in *(*B-C*)* indicate flagella where *Tb*CaCh::HA_3 is
812 absent. (D-F) *Tb*CaCh::mNG/*Tb*KHAP2/3^{RNAi} BF cell line was induced with 1 µg/ml doxycycline
813 (dox). Parasites were stained with DAPI (*blue*) and anti-*Tb*KH pAb (*Tb*KH*, red*), and mNG
814 endogenous fluorescence was also acquired (*Tb*CaCh::mNG*, green*). Parasites were induced
815 with doxycycline for (D) 0 days (*0 d dox*), (E) 4 days (*4d dox*), or (F) 7 days (*7d dox*). *Green*
816 *arrowheads* indicate flagella where *Tb*CaCh::mNG is present. Merged DIC images are
817 presented in the right panel of each image pair. The scale bar shown in (A) applies to all
818 images.
819 **Fig. 8. Trafficking of *Tb*EVMP1, *Tb*EVMP2, and *Tb*FLA1BP in *Tb*KH^{RNAi} BF parasites.** (A)
820 Parasites expressing *Tb*EVMP1:mNG before (*0 h RNAi*) and after (*24 h RNAi*) induction of RNAi
821 against *TbKH* mRNA. *Green arrowheads* indicate mNG fluorescence in the FM (all panels) or in
822 extracellular vesicles (*0 h RNAi*, right panel). *White arrowheads* indicate flagella without mNG

823 fluorescence. (B) Parasites expressing *Tb*EVMP2::mNG before (*0 h RNAi*) and after (*24 h*
824 *RNAi*) induction of RNAi against *TbKH* mRNA. (C) Parasites expressing *Tb*FLA1BP::mNG
825 before (*0 h RNAi*) and after (*24 h RNAi, 48 h RNAi*) induction of RNAi against *TbKH* mRNA. The
826 left-most images in A, B, and C represent formaldehyde fixed parasites, whereas for the other
827 images, live parasites were suspended in CyGel, which facilitates visualization of secreted
828 extracellular vesicles.
829

Figure 1

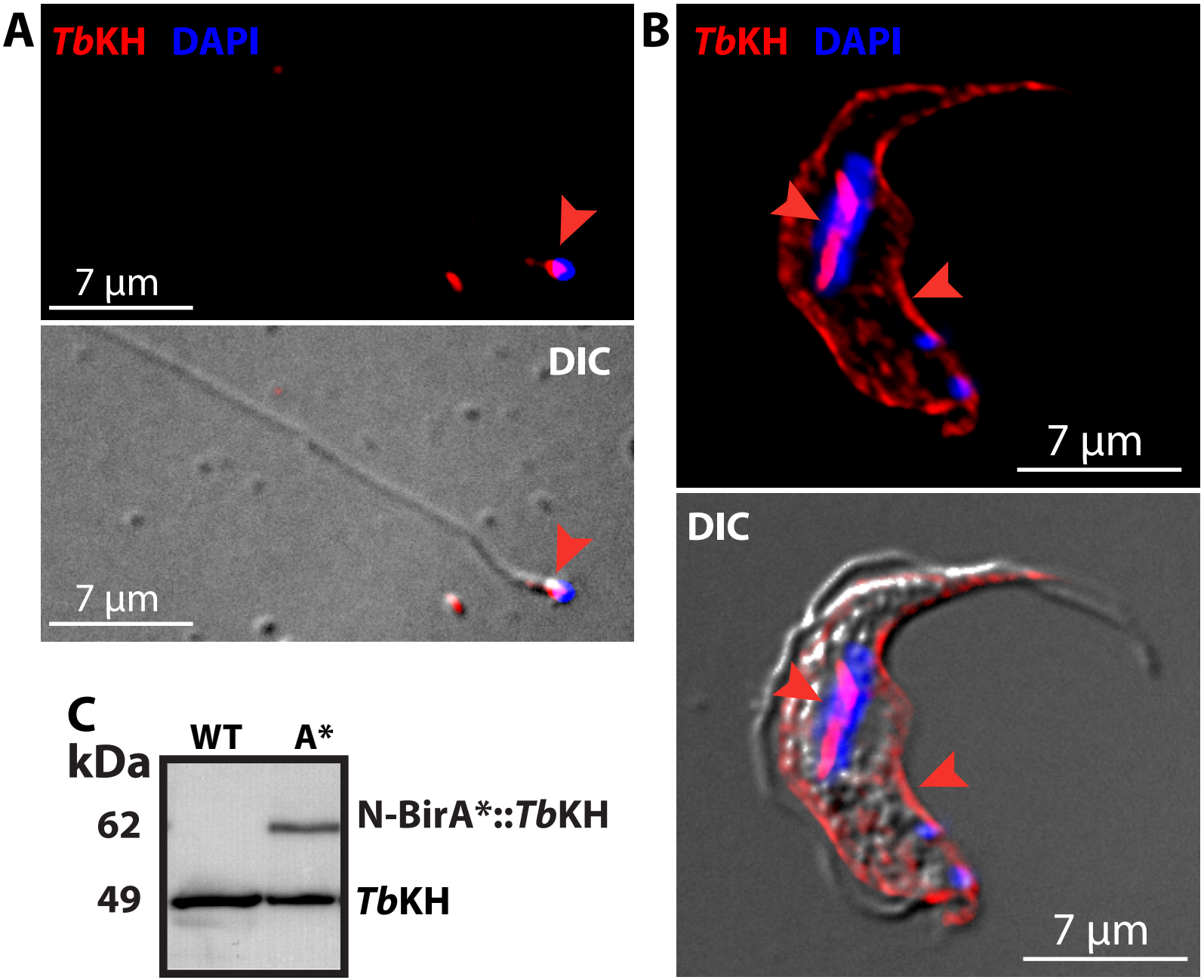
A
TbKH DAPI
7 µm
DIC
7 µm
B
TbKH DAPI
7 µm
DIC
7 µm
C
kDa
WT
A*
62
49
N-BirA*::TbKH
TbKH

Figure 2

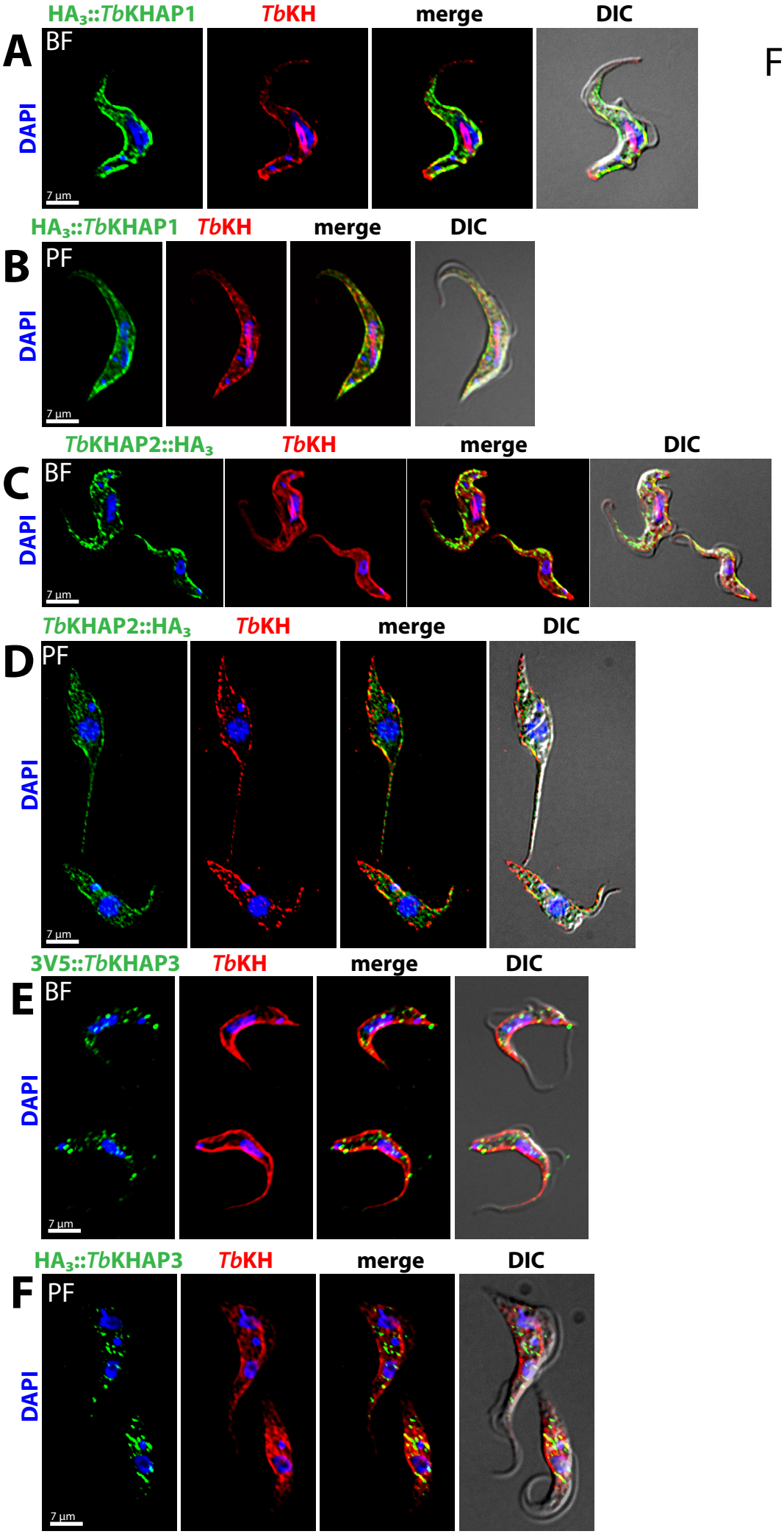
A
HA3::TbKHAP1
TbKH
merge
DIC
BF
DAPI
7 µm
B
HA3::TbKHAP1
TbKH
merge
DIC
PF
DAPI
7 µm
C
TbKHAP2::HA3
TbKH
merge
DIC
BF
DAPI
7 µm
D
TbKHAP2::HA3
TbKH
merge
DIC
PF
DAPI
7 µm
E
3V5::TbKHAP3
TbKH
merge
DIC
BF
DAPI
7 µm
F
HA3::TbKHAP3
TbKH
merge
DIC
PF
DAPI
7 µm

Figure 3

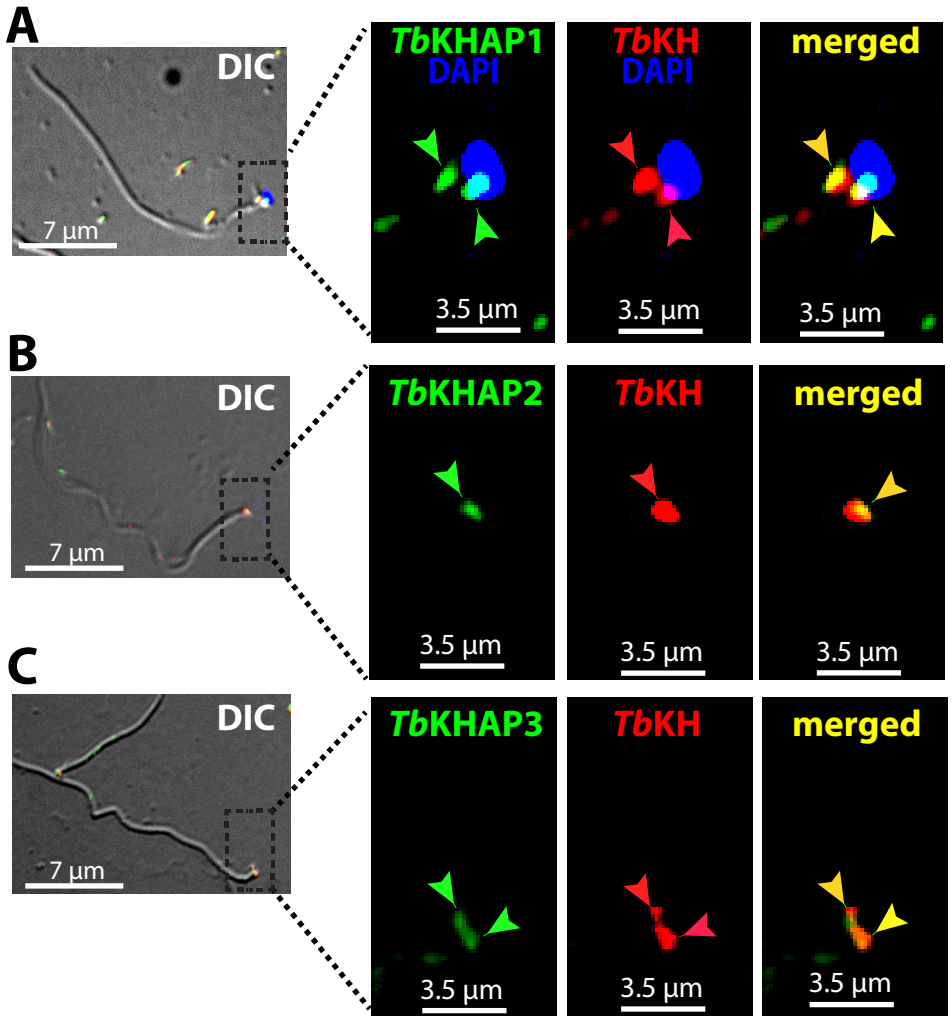
A
DIC
7 µm
TbKHAP1
DAPI
TbKH
DAPI
merged
3.5 µm
3.5 µm
3.5 µm
B
DIC
7 µm
TbKHAP2
TbKH
merged
3.5 µm
3.5 µm
3.5 µm
C
DIC
7 µm
TbKHAP3
TbKH
merged
3.5 µm
3.5 µm
3.5 µm

Figure 4

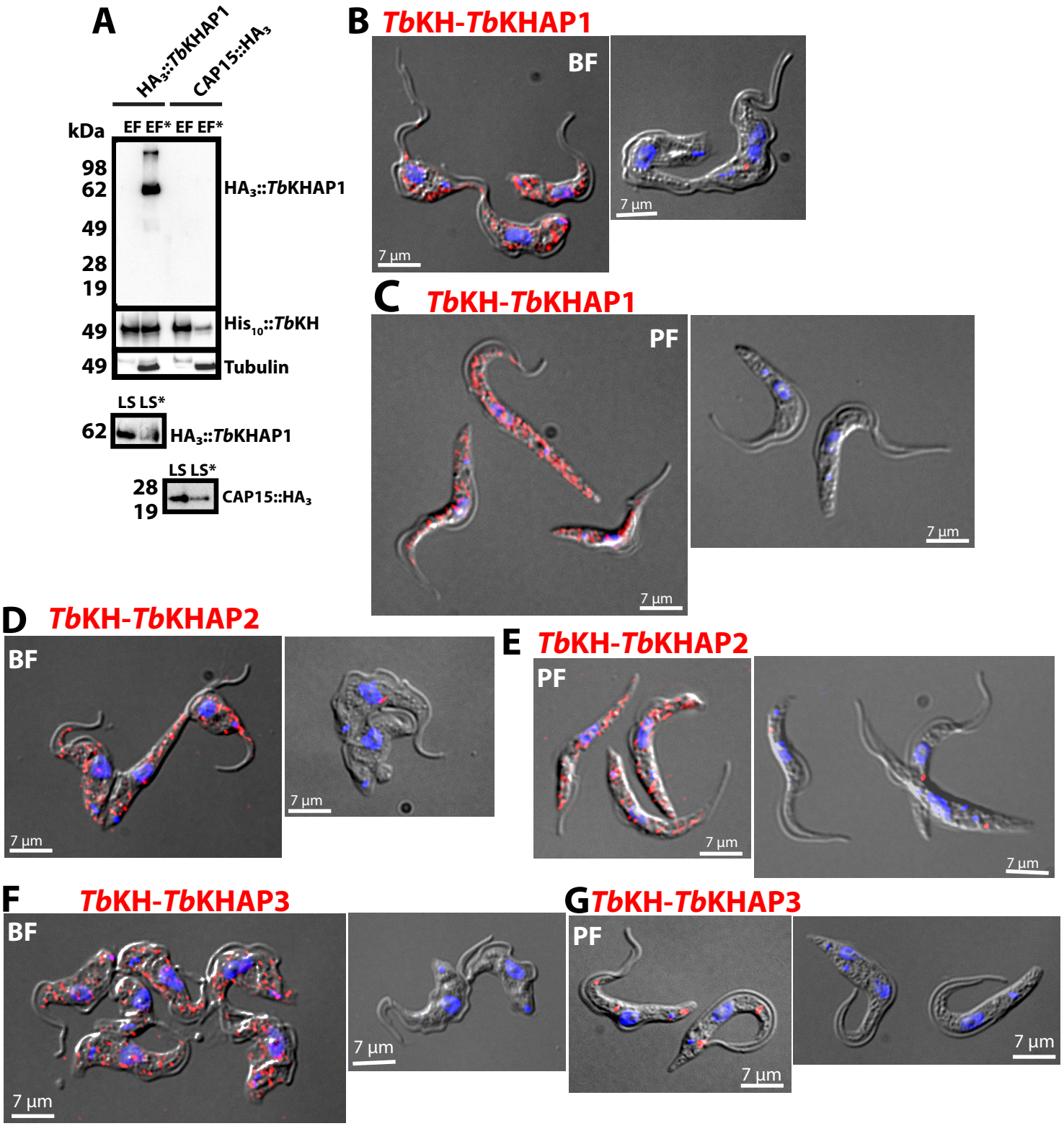
A
HA3::TbKHAP1
CAP15::HA3
kDa
EF EF* EF EF*
98
62
49
28
19
HA3::TbKHAP1
49
His10::TbKH
49
Tubulin
LS LS*
62
HA3::TbKHAP1
LS LS*
28
19
CAP15::HA3
B TbKH-TbKHAP1
BF
7 µm
7 µm
C TbKH-TbKHAP1
PF
7 µm
7 µm
D TbKH-TbKHAP2
BF
7 µm
7 µm
E TbKH-TbKHAP2
PF
7 µm
7 µm
F TbKH-TbKHAP3
BF
7 µm
7 µm
G TbKH-TbKHAP3
PF
7 µm
7 µm

Figure 5

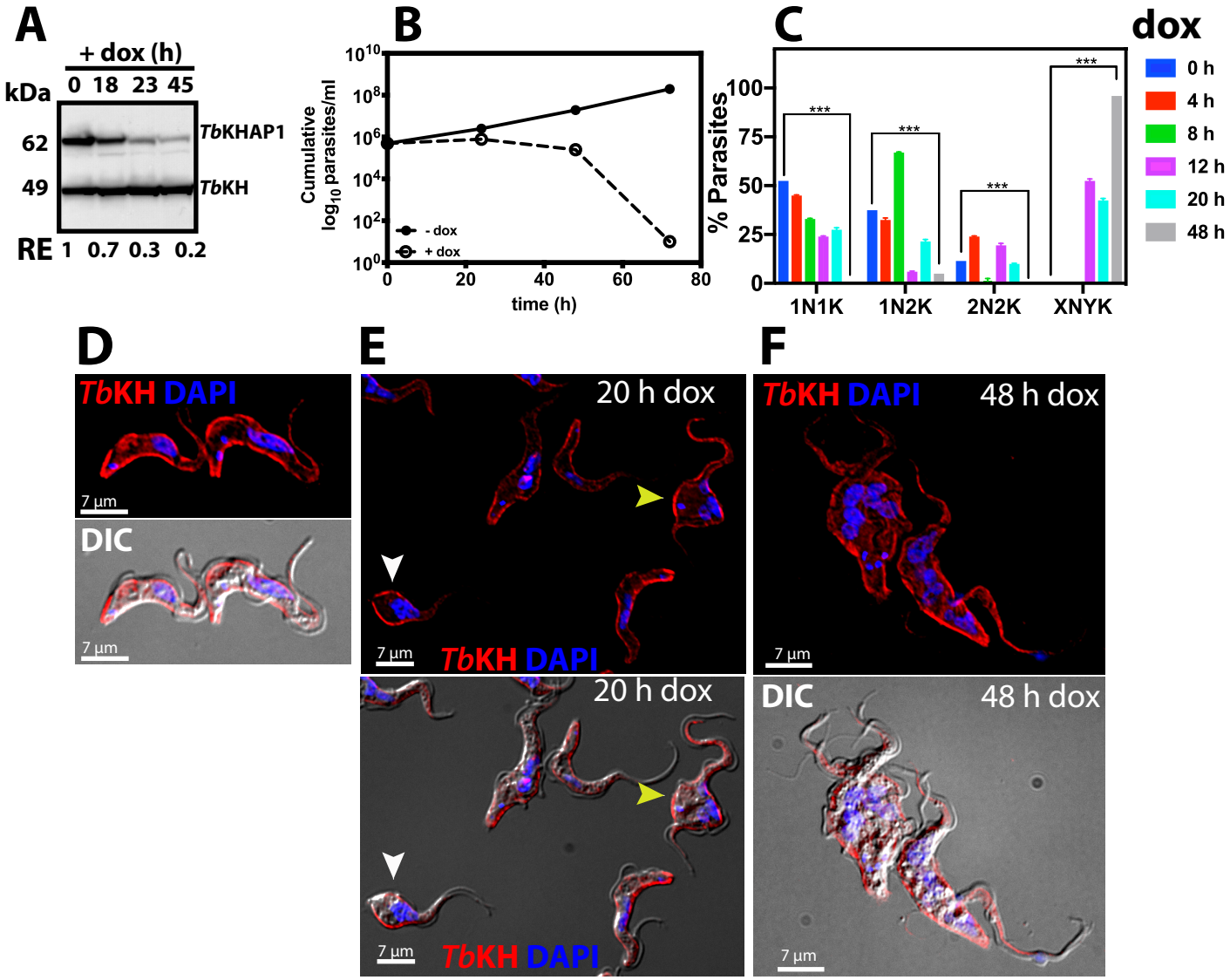
A
+ dox (h)
0 18 23 45
kDa
62
49
TbKHAP1
TbKH
RE 1 0.7 0.3 0.2
B
Cumulative log10 parasites/ml
time (h)
- dox
+ dox
C
% Parasites
1N1K
1N2K
2N2K
XNYK
dox
0 h
4 h
8 h
12 h
20 h
48 h
D
TbKH DAPI
DIC
7 µm
E
20 h dox
F
48 h dox

Figure 6

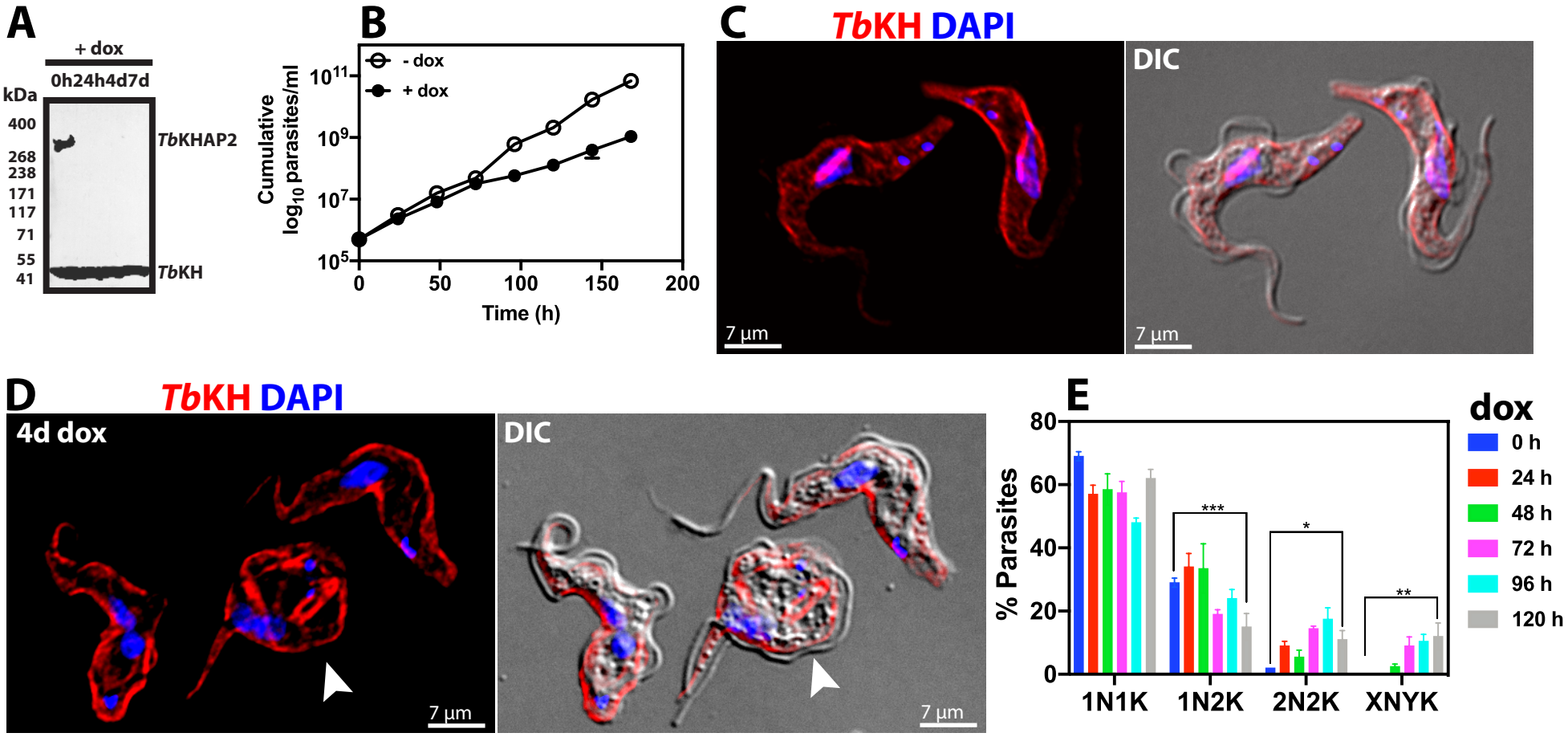
A
+ dox
0h24h4d7d
kDa
400
268
238
171
117
71
55
41
TbKHAP2
TbKH
B
- dox
+ dox
Cumulative log10 parasites/ml
10^11
10^9
10^7
10^5
0
50
100
150
200
Time (h)
C
TbKH DAPI
DIC
7 µm
7 µm
D
TbKH DAPI
4d dox
DIC
7 µm
7 µm
E
% Parasites
80
60
40
20
0
***
*
**
1N1K
1N2K
2N2K
XNYK
dox
0 h
24 h
48 h
72 h
96 h
120 h

Figure 7

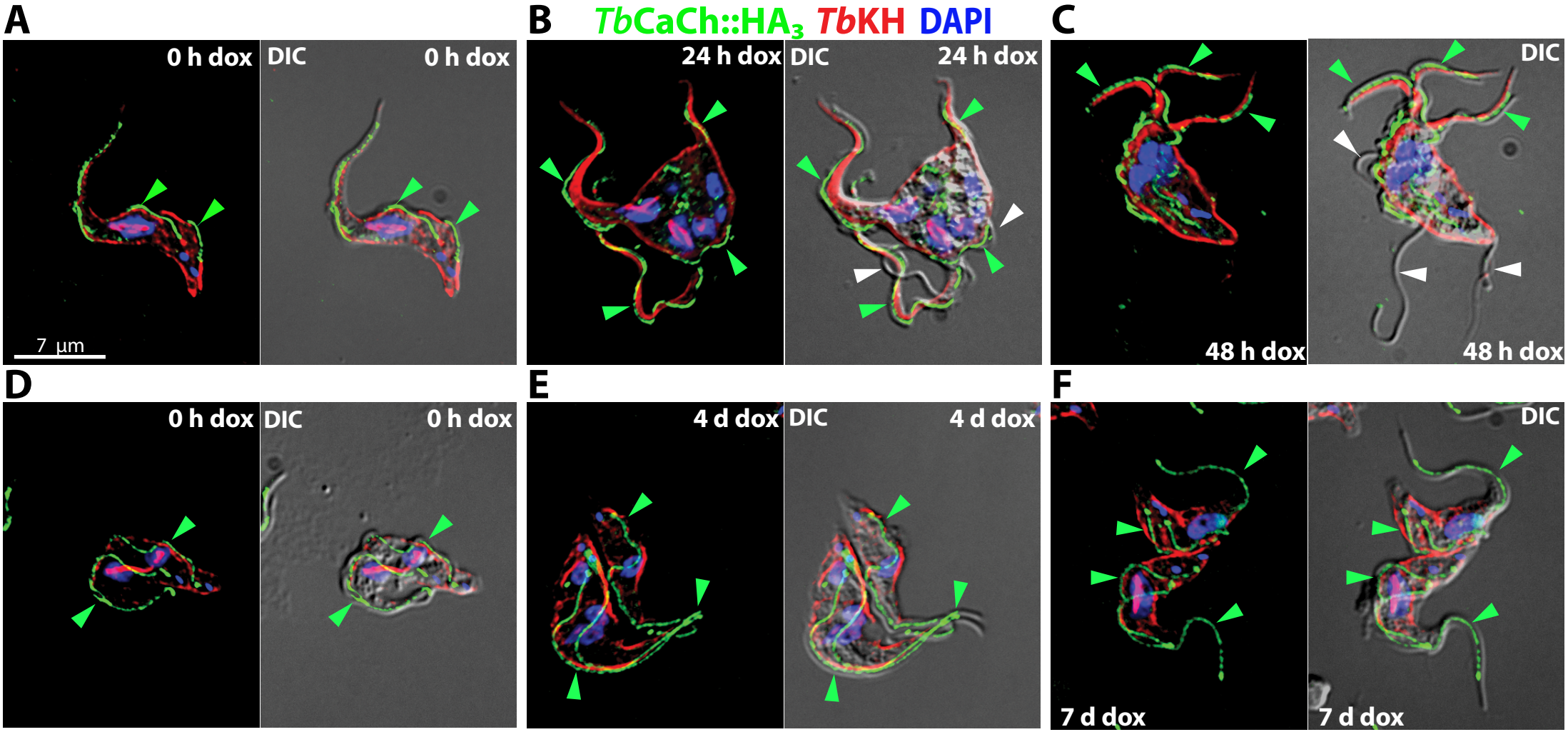
A
0 h dox
DIC
0 h dox
7 µm
B
TbCaCh::HA3 TbKH DAPI
24 h dox
DIC
24 h dox
C
48 h dox
DIC
48 h dox
D
0 h dox
DIC
0 h dox
E
4 d dox
DIC
4 d dox
F
7 d dox
DIC
7 d dox

Figure 8

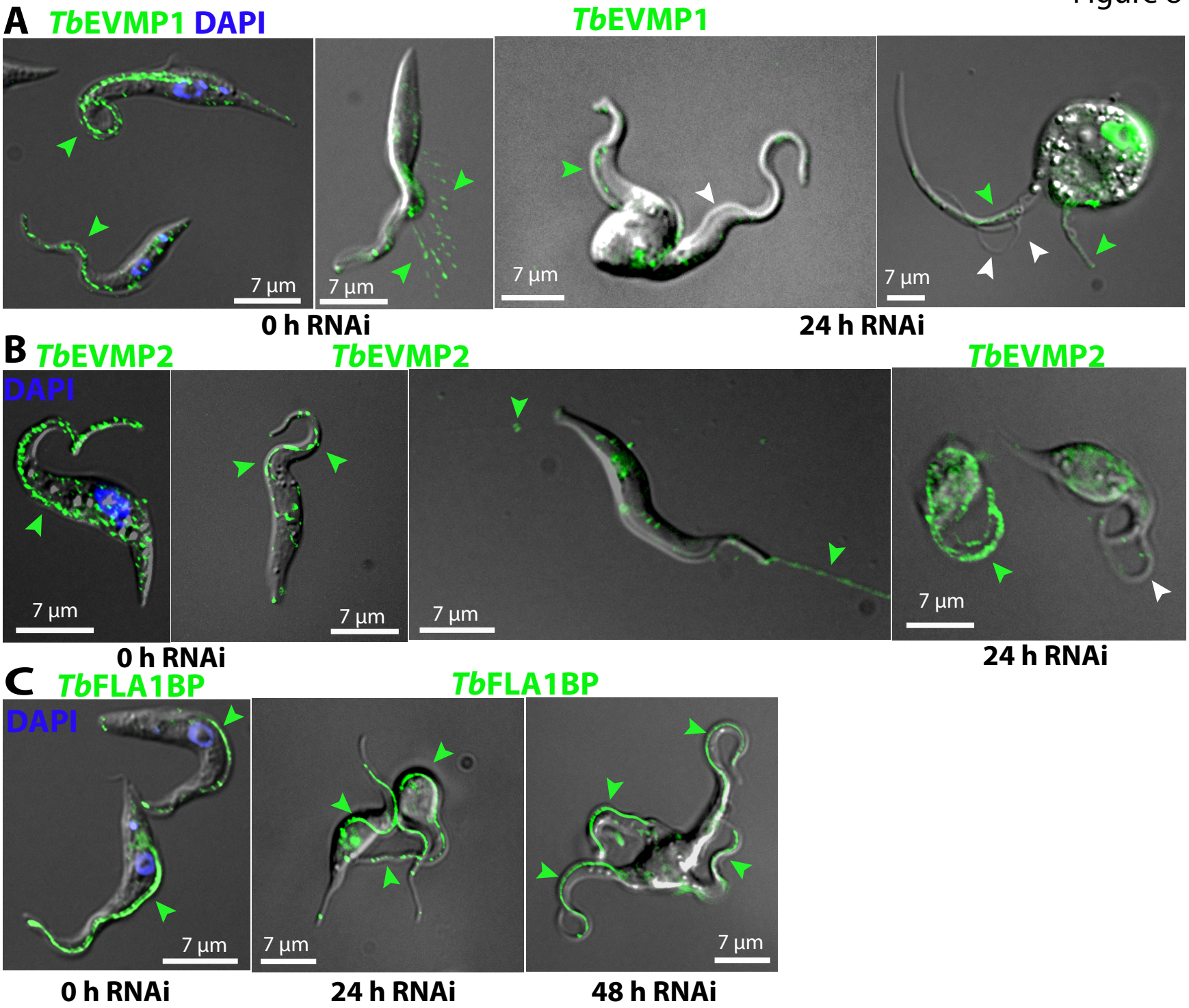
A
TbEVMP1 DAPI
TbEVMP1
7 µm
7 µm
7 µm
7 µm
0 h RNAi
24 h RNAi
B
TbEVMP2
DAPI
TbEVMP2
TbEVMP2
7 µm
7 µm
7 µm
7 µm
0 h RNAi
24 h RNAi
C
TbFLA1BP
DAPI
TbFLA1BP
7 µm
7 µm
7 µm
0 h RNAi
24 h RNAi
48 h RNAi